# Immunosuppressants Rewire the Gut Microbiome-Alloimmune Axis Through Time-Dependent and Tissue-Specific Mechanisms

Long Wu[1,2,+], Allison Kensiski[2,+], Samuel J Gavzy[1,2], Yang Song[3], Hnin Wai Lwin[3], Michael France[3,4], Dejun Kong[2], Lushen Li[1,2], Ram Lakhan[1,2], Vikas Saxena[1,2], Wenji Piao[1,2], Marina W. Shirkey[2], Valeria R Mas[1,4], Brendan Lohmar[1,2], Yan Shu[5], Jonathan S Bromberg[1,2,4]*, Bing Ma[3,4]*

[1]University of Maryland School of Medicine, Department of Surgery, Baltimore, MD, USA

[2]University of Maryland School of Medicine, Center for Vascular and Inflammatory Diseases, Baltimore, MD, USA

[3]University of Maryland School of Medicine, Institute for Genome Sciences, Baltimore, MD, USA

[4]Department of Microbiology and Immunology, University of Maryland School of Medicine, Baltimore, MD, USA

[5]Department of Pharmaceutical Sciences, University of Maryland School of Pharmacy, Baltimore, MD, USA

[+]Authors contributed equally to this work

*Corresponding Authors:

Jonathan S. Bromberg, MD, PhD jbromberg@som.umaryland.edu

Bing Ma, PhD bma@som.umaryland.edu

Keywords: immunology, immunosuppressants, gut dysbiosis, microbiome, metabolome

## Abstract

**Background**:

Lifelong immunosuppressive therapy is required to prevent allograft rejection in organ transplantation. Current immunosuppressants effectively suppress adaptive and innate immune responses, but their broad, antigen-non-specific effects often result in severe off-target complications. It remains a significant unmet medical need in transplant medicine.

**Results:**

In this study we investigated immunosuppressant effects of four major immunosuppressant classes, including tacrolimus, prednisone, mycophenolate mofetil (MMF), and fingolimod (FTY), on the gut microbiome, metabolic pathways, lymphoid architecture and lymphocyte trafficking after up to 30-day chronic exposure. Despite their distinct mechanisms of action and not designed to target the gut, all immunosuppressive drugs induced profound and time-dependent alterations in both intestine gene expression and gut microbiome composition. Progressive alterations from moderate early, drug-specific changes to a strikingly convergent microbial dysbiosis, marked by significant expansion of pathobionts of *Muribaculaceae*, occurred across all drug classes. Concurrently, all drugs uniformly induced significant suppression of mucosal immunity including B cell, immunoglobulin, and antigen recognition. Time-dependent changes in lymph node (LN) reorganization and cellular composition were also observed, marked by a progressive shift toward pro-inflammatory phenotypes in gut-draining mesenteric LNs and a gradual loss of tolerogenic architecture in peripheral LNs. Drug-specific metabolic alterations and distinct phases of

intestinal transcriptional responses were also characterized. Notably, MMF and FTY demonstrated the most robust immunomodulatory properties, and were able to suppress alloantigen-induced inflammation through mediating regulatory T cell distribution and LN remodeling.

**Conclusions:**

Together, these findings highlight the underappreciated complexity and temporal dynamics immunosuppressants effects, particularly their impact on the gut and compartmentalized regulation of alloimmune in lymphoid tissues. Understanding these relationships offers new opportunities for refining immunosuppressive strategies to reduce treatment-related off-target complications and improve long-term organ transplant outcomes.

60 **Introduction**

61 Prevention of solid organ transplant rejection necessitates lifelong, multimodal
62 immunosuppression to dampen both adaptive and innate alloreactive immunity. Despite
63 improved short-term outcomes, long-term graft survival remains suboptimal due to
64 chronic rejection and a range of adverse events such as metabolic complications,
65 infections, neoplasia, and organ-specific toxicities [1-8]. Current immunosuppressants
66 target specific immune pathways but are limited by their antigen-non-specific nature,
67 broadly suppressing the immune system and causing off-target effects [9,10]. This
68 dilemma between necessary immunosuppression and its imprecise, system-wide
69 effects represents a critical challenge for improving long-term transplant outcomes.
70

71 A comprehensive understanding of the effects of immune suppressant drugs is
72 essential for optimizing therapeutic regimens, minimizing adverse events, and
73 preventing graft rejection. While most mechanistic studies on immunosuppressants
74 have focused on their effects on T cells, B cells, and dendritic cells (DCs), little is known
75 about their impact on secondary lymphoid organs (SLOs), particularly lymph nodes
76 (LNs). As key regulators of local and systemic immunity, LNs direct immune responses
77 toward tolerance or activation, with their function critically dependent on the architecture
78 maintained by lymph node stromal cell (LNSC) networks, including fibroblastic reticular
79 cells (FRCs), lymphatic endothelial cells (LECs), and blood endothelial cells (BECs).
80 LNSCs orchestrate the positioning and interaction of lymphocytes with antigen-
81 presenting cells (APCs) like DCs through the coordinated action of chemokines,
82 cytokines, and stromal fibers [11-13]. FRC-derived laminins are particularly important, as

83 the laminin α4:α5 ratio (La4:La5) within the T cell cortex of the cortical ridge (CR) and
84 around high endothelial venules (HEVs) modulates the balance between tolerance and
85 immunity and influences global immune states [14,15]. An increased La4:La5 promotes a
86 pro-tolerogenic environment, whereas a decreased ratio fosters inflammation. LN
87 structure and FRC function are often disrupted during transplantation due to ischemia-
88 reperfusion injury (IRI) to the graft, leading to persistent “immunologic scarring”, a
89 pathologic alteration of the LN cellular network [16,17]. Further, regulatory T cells (Tregs)
90 do not simply suppress immune responses through their presence alone. Their precise
91 localization within LNs is critical for maintaining immune homeostasis. Tregs around
92 HEVs limit the entry of pro-inflammatory effector T cells into the LNs. This gatekeeping
93 function helps maintain a tolerogenic environment by preventing excessive
94 accumulation of pro-inflammatory cells [14]. Tregs in the CR suppress T cell priming and
95 activation by APCs, preventing effector T cell activation and differentiation [18]. A
96 reduction of Tregs in these regions can result in enhanced T cell activation, promoting a
97 pro-inflammatory state [19-21]. Despite the importance of LN architecture and Treg
98 localization in immune modulation, the effects of immunosuppressive drugs on these
99 structural and functional elements remain poorly understood. Addressing this gap is
100 critical for developing strategies to enhance long-term allograft survival.
101
102 Beyond their immunomodulatory effects, immunosuppressive drugs profoundly
103 influence gut microbiome composition and function, which has been significantly
104 implicated in alloimmunity and graft survival [22-27]. Our group has demonstrated that gut
105 microbiota modulates LN architecture by altering stromal fiber laminins [28-30]. Our recent

106 studies of tacrolimus and the mammalian target of rapamycin (mTOR) inhibitor
107 rapamycin have revealed broad effects of these drugs on gut microbiome, luminal
108 metabolic functions, intestinal transcriptome, as well as LN architecture [31,32], consistent
109 with previous studies [33,34]. This work suggests a crucial mechanistic link between gut
110 microbiota and immune regulation. Other research has shown diverse mechanisms by
111 which immunosuppressants affect host-microbe interactions. For example,
112 methotrexate inhibits the conserved dihydrofolate reductase pathway in both host and
113 gut bacteria, leading to broad microbiome alterations [35], while certain
114 immunosuppressants disrupt the intestinal barrier, altering intestinal permeability [36].
115 Notably, these host-microbe interactions are bidirectional, as gut microbiota can also
116 alter intestinal function and drug bioavailability [37,38]. For example, mycophenolate
117 mofetil (MMF) is metabolized to inactive glucuronidated mycophenolic acid (MPAG) via
118 hepatic glucuronidation, and luminal bacteria expressing β-glucuronidase can reactivate
119 the metabolized form MPAG back to active MPA, leading to increased concentrations of
120 active luminal drug and colonic inflammation [39]. These complex interactions among
121 immunosuppressants, gut microbiota, intestinal function, and immune cell populations
122 underscore the need for a comprehensive understanding of their interrelationships to
123 optimize therapeutic efficacy and mitigate unintended effects.
124
125 In this study, we investigated the understudied effects of immunosuppressants on LN
126 architecture, lymphocyte and myeloid cell distribution, and the gut microbiome. We
127 examined four key classes of clinical immunosuppressants: the calcineurin inhibitor
128 tacrolimus (TAC), the glucocorticoid prednisone (PRED), the inosine monophosphate

129 dehydrogenase (IMPDH) inhibitor MMF, and the sphingosine-1-phosphate (S1P)
130 receptor antagonist fingolimod (FTY). Our findings revealed complex, time-dependent
131 and tissue-specific patterns in drug responses and strikingly convergent gut microbial
132 and intestinal responses. Despite their distinct mechanisms of action and not designed
133 to target the gut, all drugs induced progressive alterations from moderate early changes
134 to substantial alterations with prolonged treatment, converging to a shared dysbiotic
135 state in the gut microbiome marked by significant expansion of pathobionts of
136 *Muribaculaceae* across all drug classes. This was accompanied by significant metabolic
137 alterations and distinct phases of intestinal transcriptional responses. Time-dependent
138 changes were also observed in LNs. The mesenteric LNs (mLNs) developed
139 progressively increased pro-inflammatory states with extended immunosuppressive
140 use, while peripheral LNs (pLNs) showed strong early pro-tolerogenic effects that
141 became less pronounced over time. While this compartmentalized immune regulation
142 was broadly consistent across all drugs studied, MMF and FTY demonstrated
143 particularly robust immunomodulatory effects. These two agents effectively suppressed
144 alloantigen-induced pro-inflammatory changes, through mediating Treg redistribution
145 and LN remodeling. Overall these findings revealed the underappreciated complexity
146 and dynamics of immunosuppressant effects, suggesting a mechanistic link between
147 immunosuppressant-induced gut dysbiosis, compartmentalized immune regulation in
148 peripheral and mesenteric lymphoid tissues, and immunosuppressant off-target
149 complications.

150 **Results**

151 Time-dependent effects of immunosuppressants on gut microbiome

152 We treated groups of C57BL/6 mice daily with four immunosuppressants (TAC, PRED,
153 MMF and FTY), respectively, using untreated mice as controls. We analyzed the gut
154 microbiome at early (3 days), intermediate (7 days), and late (30 days) time points. We
155 performed whole community metagenomic sequencing on colonic intraluminal stool
156 samples and utilized the comprehensive mouse gut metagenome catalogue (CMGM) [40]
157 (**Supplemental Table 1A**) for taxonomic profiling and Human Microbiome Project
158 Unified Metabolic Analysis Network (HUMAnN3) [41] (**Supplemental Table 1B**) to
159 analyze microbial metabolic pathways.

160

161 To quantify immunosuppressant drug effects on the gut microbiome, we used Bray-
162 Curtis distance analyses to measure changes in both taxonomic composition and
163 metabolic pathways (**Figure 1A, B**). We compared each treatment group to untreated
164 controls (treatment-to-control) to determine deviations from baseline and analyzed
165 differences between different treatment groups (treatment-to-treatment). In treatment-to-
166 control pairwise comparisons, the effects were variable during early treatment by day 3
167 and 7. However, by day 30, all treatment groups showed profound and significant
168 alterations in their gut microbiome profiles, suggesting a cumulative drug effect with
169 prolonged treatment. The pattern was evident in both taxonomic compositions and
170 functional pathways, with the most substantial changes emerging with 30-day treatment.
171 Drug-to-drug pairwise comparison also revealed distinct time-dependent drug effects on
172 gut microbiome. The differences between treatment groups increased from day 3 to

173 day 7, indicating drug-specific early effects on microbial communities. However, by day
174 30, these inter-drug differences had substantially decreased, suggesting that despite
175 their distinct mechanisms of action, prolonged immunosuppression lead to convergent
176 effects on the gut microbiome. These findings were further supported by ordination
177 analyses. Principal Component Analysis (PCA) revealed clear clustering of 30-day
178 samples, distinct from earlier time points, regardless of the specific immunosuppressant
179 used (**Figure 1C**). Canonical Correspondence Analysis (CCA) confirmed these
180 observations, demonstrating significant correlations between treatment duration and
181 microbiome composition, with maximal separation occurring at 30 days (**Supplemental**
182 **Figures 1A and 1B**).
183
184 The temporal convergence of microbiome alterations across different
185 immunosuppressant drugs revealed shared downstream influences of these drugs on
186 host-microbe interactions, despite their diverse initial effects. To identify microbial
187 signatures associated with immunosuppression, we compared the abundance of
188 bacterial species between drug-treated and control groups across multiple timepoints to
189 reveal treatment-specific and temporal changes in microbial populations (**Figure 1D**).
190 No individual taxonomic group showed consistent alterations across all timepoints in
191 any treatment group. Early (day 3) and intermediate (day 7) time points revealed
192 sporadic alterations in various bacterial taxa, but these changes were transient. By day
193 30, all treatment groups, despite their distinct mechanisms of action, converged on a
194 common set of bacterial taxa that were not significant at the earlier time points. These
195 taxa belonged exclusively to the family of *Muribaculaceae* (formerly known as *S24-7*),

196 including *Duncaniella*, *Paramuribaculum intestinale*, and *CAG-873*. This family is known
197 for its metabolic versatility and adaptability [42-44], and is primarily a gut commensal in
198 mice but can act as pathobionts under dysbiotic conditions, with recent evidence
199 demonstrating their causative role in insulin-dependent diabetes in mouse models [45].
200 Their enrichment indicates a shift toward a dysbiotic state in which the microbial
201 balance is skewed toward species with pathobiont potentials with altered metabolic
202 capabilities. This progression from early drug-specific changes to a convergent dysbiotic
203 state with prolonged treatment underlines the profound and progressive impact of
204 chronic immunosuppressant use on the gut microbiome.

205 Conserved intestinal responses to immunosuppressants revealed induction of epithelial
206 stress and suppression of lymphoid signatures

207 To understand host gut responses to drug treatment, we analyzed the transcriptome of
208 small intestine at days 7 and 30, as these time points corresponded to significant
209 alterations in the gut microbiome during treatments. Differentially expressed genes
210 (DEGs) were identified by comparing each drug treatment group to the no-treatment
211 controls (**Supplemental Table 2A**). DEGs analysis revealed that 30-day treatments
212 induced 1.3 to 2 times more DEGs than 7-day treatments (**Figure 2A**), indicating that
213 prolonged immunosuppression triggered more extensive transcriptional changes. At day
214 7, FTY induced the largest number of DEGs. By day 30, both FTY and PRED showed
215 stronger effects in both upregulation and downregulation of DEGs. In contrast, MMF
216 showed the least impact, particularly in upregulated DEGs. TAC induced the largest
217 portion of upregulated DEGs with twice as many upregulated DEGs as downregulated
218 ones, compared to other drugs that showed either greater downregulation or balanced

219 regulation. Overall, prolonged immunosuppressive treatment drove broader and more
220 extensive transcriptional changes in intestinal tissue.
221
222 We next analyzed DEGs common to all immunosuppressant treatments to identify
223 shared drug-induced effects (**Supplemental Table 2B-D**). To enable a comprehensive
224 comparison across different immunosuppressant classes, we integrated transcriptomic
225 data from rapamycin-treated mice from our previously study [31] into the current analysis
226 (**Figure 2B**). Conserved DEGs were defined as genes consistently differentially
227 expressed by at least four drugs at either time points. Clustering analysis of these
228 conserved DEGs at days 7 and 30 revealed distinct temporal expression patterns,
229 particularly affecting genes involved in mucosal immunity, epithelial homeostasis,
230 metabolism, and circadian regulation (**Figure 2C**).
231
232 Specifically, immunoglobulin heavy variable (Ighv) and kappa light chain variable (Igkv)
233 region genes displayed broad yet temporally distinct responses under
234 immunosuppressant treatments. Cluster 1 DEGs (**Figure 2B** left panel) includes genes
235 mainly suppressed at day 30, including classical Ighv and Igkv segments typically
236 associated with naive and T-dependent germinal center-derived B cells. This
237 downregulation indicates a significant, prolonged suppression of *de novo* B cell
238 activation and diversification, especially affecting clones that require antigen-specific, T
239 cell-dependent signals. Cluster 2 DEGs were mostly suppressed at day 7 only. These
240 genes, which include variable region segments commonly expressed by naive or early
241 responding B cells, suggest an early transcriptional quiescence. In contrast, Cluster 3

242 genes were initially suppressed at day 7 but later upregulated at day 30. The activation
243 of the Ighg2b gene suggests that class-switch recombination has occurred, reflecting
244 the selective survival and expansion of mucosal or microbiota-tolerant B cell subsets
245 capable of adapting to the chronically immunosuppressed gut. Overall, these results
246 indicate a predominantly suppressed B cell transcriptional program, with limited
247 recovery by day 30.
248
249 Further immunohistochemical (IHC) assessments of intestinal conventional dendritic
250 cells (CD11c+ cDCs) and regulatory T cells (Foxp3+ Tregs) revealed day 7 was the
251 critical transitional point for all immunosuppressant drugs (**Supplemental Figure 2A-C**).
252 A significant reduction in intestinal cDC populations at day 7 was observed for all drugs,
253 with no significant alterations observed at days 3 or 30. Intestinal Tregs similarly had the
254 most significant decreases at day 7, while returning to baseline levels by day 30.
255 Collectively, these results indicated that at day 7, B cells experienced diminished
256 antigenic stimulation, reduced survival and differentiation signals, and suppressed
257 transcription of immunoglobulin variable region genes. By day 30, limited restoration of
258 antigen delivery, B and T cell costimulatory signals, and epithelial tolerance to baseline
259 levels associated with partial resumption of recombined immunoglobulin gene
260 transcription, especially among surviving tissue-resident B cells. This partially restored
261 yet still broadly suppressed state may represent a compensatory host response,
262 favoring class-switched memory or microbiota-reactive B cell clones to maintain
263 mucosal homeostasis under ongoing immunosuppressive therapy.
264

265 Epithelial DEGs showed three distinct temporal expression clusters, reflecting the
266 mucosal defense and host compensatory responses to immunosuppressant treatment.
267 Cluster 1 DEGs were significantly activated by day 30, indicative of robust mucosal
268 defense mechanisms and adaptive metabolic programs. Outstandingly, this cluster
269 included key antimicrobial effectors, including $\alpha$-defensins (Defa-ps16, Defa-ps7, Defa2,
270 Defa20-22, Defa29, Defa3, Defa32, Defa34-36, Defa40-42, Defa5), lysozyme (Lyz1),
271 and secretory phospholipase A2 group IIA (Pla2g2a), which are canonical products of
272 Paneth cells [46]. This transcriptional profile is consistent with a Paneth cell-driven
273 antimicrobial response, suggesting that activation of innate epithelial defense
274 mechanisms was possibly triggered by pathobiont expansion and microbiota
275 perturbation following prolonged immunosuppressant exposure. Further, oxidase genes
276 (Duox2, Duoxa2) were elevated, supporting reactive oxygen species (ROS) production
277 for microbial control. Moreover, upregulation of inducible nitric oxide synthase (iNOS,
278 Nos2) and glutathione peroxidase (Gpx2) suggested enhanced epithelial stress
279 responses. These adaptive responses likely represented host mechanisms to control
280 potential microbiota perturbations. Cluster 2 genes, mainly upregulated at day 7,
281 prominently included key circadian regulators (Ciart, Per1, Per2, Per3, Hlf), suggesting
282 an early host-driven resetting of circadian rhythms in response to drug-induced gut
283 perturbation. Further, genes involved in xenobiotic metabolism and detoxification
284 pathways (Cyp26b1, Ces1d, Sult6b2) and early immune interaction genes (Cd19,
285 Fcer2a, Pax5) were also significantly induced. Together these genes represented an
286 early epithelial, metabolic and immune adaptation to drug disturbance. Cluster 3 genes
287 were downregulated at day 30, including key genes involved in epithelial differentiation

288 and renewal (Onecut2, Tmem229b), lipid biosynthesis (Srebf1), extracellular matrix
289 remodeling (Chst3, Adamts4), and mast cell proteases (Mcpt1, Cma2). The suppression
290 of these functions reflected a compromised capacity for epithelial regeneration and
291 reduced structural adaptability after prolonged treatment. Overall, these data showed a
292 profound off-target influence of the immunosuppressant drugs on the intestine, and
293 importantly, a dynamic mucosal adaptation to immunosuppressive induction,
294 transitioning from initial circadian and xenobiotic metabolism, progressing toward robust
295 innate mucosal defense programs and suppression of epithelial renewal and structural
296 remodeling processes.

297 Drug-specific alterations in intestinal expression and gut luminal metabolic activity

298 Beyond shared mechanisms, we next examined drug-specific transcriptional programs
299 to identify unique intestinal responses elicited by individual immunosuppressant agents.
300 UpSet plots were used to analyze DEGs unique to or shared between days 7 and 30, as
301 well as across different treatment groups (**Supplemental Figure 3A-D**). Drug effects
302 were more pronounced at day 30, with 1.6-3.3 times more down-regulated DEGs and
303 1.4-2.2 times more upregulated DEGs compared to day 7. Among the treatments, TAC
304 showed the most pronounced effect at day 30, while FTY had the least impact. Further,
305 minimal overlap in DEGs was observed between timepoints and across different
306 treatments, indicating transient effects at day 7. For instance, following PRED
307 treatment, only 31 genes (15 upregulated, 16 downregulated) were consistently
308 modulated at both timepoints, while 255 genes were uniquely regulated at day 7 (81
309 upregulated, 78 downregulated) and 371 at day 30 (174 upregulated, 197
310 downregulated). This pattern held true for all four drug treatments. Further comparison

311 between treatment groups revealed distinct patterns of gene expression (**Supplemental**
312 **Figure 4A-B**). The overlap in DEGs was limited, with less than 20% between any two
313 drugs and less than 5% across the four drugs, underscoring highly drug-specific
314 mechanisms of action on intestine. Together, these findings demonstrated that
315 immunosuppressants induced time-dependent intestinal responses, with most
316 pronounced drug-specific changes following prolonged treatment.
317
318 Gene ontology enrichment analyses of DEGs revealed drug-specific patterns
319 (**Supplemental Figure 4C**). At day 7, FTY showed the strongest suppressive effect on
320 mucosal and humoral immunity pathways, which transitioned to moderate activation of
321 immunoglobulin production by day 30. MMF shifted from early activation on day 7 to
322 broad suppression of innate immune pathways at day 30. TAC showed moderate
323 increases in lymphocyte and immunoglobulin pathways at day 7, progressing to
324 stronger activation of both innate immunity and antibody production at day 30. PRED
325 maintained relatively modest effects throughout the treatment period, though the
326 specific pathways affected differed between the two timepoints. Together, these data
327 demonstrated that immunosuppressant drugs exerted both shared and drug-specific
328 effects on the intestine, profoundly impacting epithelial function as well as innate and
329 adaptive immune pathways, contributing to the off-target effects of immunosuppressive
330 therapies.
331
332 Gut luminal metabolic activity of small intestine was further analyzed at day 7, as this
333 time point represented a critical transitional phase. Untargeted metabolomic analysis

334 identified 264 distinct metabolites in intraluminal stool samples (**Supplemental Table**
335 **3A-B**). Partial Least Squares Discriminant Analysis (PLS-DA) demonstrated separations
336 of metabolic profiles among the different treatment groups (**Supplemental Figure 5A**),
337 and the top contributing metabolites in each group are shown in **Supplemental Figure**
338 **5B**. Hierarchical clustering analysis further confirmed these drug-specific patterns,
339 demonstrating that each immunosuppressant induced unique changes in metabolite
340 abundance (**Supplemental Figure 5C**). Pairwise comparison of individual drugs to no-
341 treatment controls, combined with enrichment analyses, revealed both shared and drug-
342 specific effects on metabolic activities (**Table 1**, **Supplemental Table 3C-F**).
343
344 TAC treatment induced similar numbers of significantly increased and decreased
345 metabolites (**Supplemental Figure 6A, Supplemental Table 3F**). Metabolites elevated
346 by TAC included amino acids and derivatives, suggesting altered protein catabolism
347 and amino acid utilization; pyrimidine metabolites indicative of increased nucleotide
348 turnover, and sugars/sugar phosphates reflecting enhanced glycolytic activity and
349 central carbon metabolism. Conversely, TAC significantly reduced polyamines, biogenic
350 amines, short-chain fatty acids (SCFAs), betaine, trimethylamine (TMA), and various
351 organic acids. In contrast, PRED, MMF, and FTY primarily induced suppressive
352 metabolic effects, each with distinct scope and profiles. PRED caused the broadest
353 suppression, reducing three to four times more metabolites than it increased
354 (**Supplemental Figure 6B, Supplemental Table 3D**), including amino acid derivatives,
355 SCFAs, TMA, pyrimidine intermediates, and polyamines, consistent with its widespread
356 inhibitory effects on cellular metabolism [47-49]. MMF showed a similarly suppressive but

357 more targeted profile, predominantly affecting glyoxylate/dicarboxylate metabolism,
358 branched-chain and aromatic amino acids, and purine pathways (**Supplemental Figure**
359 **6C, Supplemental Table 3E**). MMF increased adenosine while reducing uric acid,
360 consistent with its mechanism as an inosine monophosphate dehydrogenase (IMPDH)
361 inhibitor [50,51], directly linking metabolic changes to its therapeutic effects. FTY induced a
362 relatively milder suppressive profile (**Supplemental Figure 6D, Supplemental Table**
363 **3C**), with increased nucleosides and reduced nucleotides and SCFAs. Notably,
364 decreased arginine and elevated $N^1$,$N^8$-diacetylspermidine and spermidine pointed to
365 enhanced polyamine biosynthesis. Collectively, these findings underscore shared and
366 distinct metabolic alterations in the gut lumen that may contribute to both therapeutic
367 efficacy and off-target effects.

368 Tissue-specific and time-dependent effects of immunosuppressants on mLN and pLN
369 organization

370 We next investigated how immunosuppressants affected LN organization in both
371 mucosal and systemic compartments by examining mLN and pLN, the primary draining
372 sites for mucosal and systemic immunity, respectively. IHC provides spatial resolution,
373 enabling localized assessments of Tregs within special areas such as LN HEVs and
374 CRs, whereas flow cytometry offers a quantitative measurement of overall Treg
375 populations. These methods complemented each other, measuring different aspects of
376 immune cell dynamics and distribution. Using flow cytometry and IHC, we analyzed
377 changes in the numbers and distribution of immune cell populations (B220+ B cells,
378 CD4+ T cells, CD8+ T cells, Foxp3+ Tregs) and structural features (La4:La5 in LNs).
379 We particularly assessed the changes to La4:La5 and distribution of Tregs in the CR

380 and around the HEVs of LNs to understand how immunosuppressants modulated
381 cellular and structural aspects of immune organization crucial for immune regulation.
382
383 In mLNs, flow cytometry revealed that B220+ B cells, CD4+ T cells, CD8+ T cells and
384 Foxp3+ Tregs were unaffected by TAC or MMF treatment at days 3, 7, or 30; in
385 contrast, PRED treatment significantly reduced CD4+ T cells and B220+ B cells by day
386 30, with no significant changes at earlier time points (**Figure 3A, C**). FTY treatment
387 increased Foxp3+ Tregs by day 30, with no changes at days 3 or 7 (**Figure 3B, C**).
388 Overall, while CD8+ T cell populations did not significantly change across conditions
389 (data not shown), other populations showed treatment-specific changes that were only
390 evident after prolonged treatment. IHC revealed two groups of change patterns. On the
391 one hand, TAC and PRED showed no significant changes in Treg distribution at any
392 time point (**Figure 3D, E, H, I, Supplemental Figure 6A, B**), but reduced La4:La5
393 around the CR after 30 days (**Figure 3F, H, Supplemental Figure 6C**). TAC
394 additionally decreased this ratio in the HEV on day 7 (**Figure 3G, I, Supplemental**
395 **Figure 6D**). On the other hand, MMF and FTY showed similar patterns with an
396 increased Treg distribution in the CR by day 7, followed by a decrease by day 30
397 (**Figure 3D, H, Supplemental Figure 6A**) and a decreased La4:La5 in both CR and
398 HEV (**Figure 3F-I, Supplemental Figure 6C, D**). Early responses at day 3 were mixed,
399 suggesting initial variable effects converged to a stable state with prolonged drug
400 treatment. Overall, despite their distinct mechanisms of action, all four
401 immunosuppressant drugs ultimately induced a more pro-inflammatory environment in
402 mLN by day 30, characterized by reduced Treg presence and/or decreased La4:La5.

403 This temporal progression suggested that prolonged immunosuppression may
404 paradoxically create localized pro-inflammatory conditions in mucosal-associated
405 lymphoid tissues.
406
407 In pLNs, distinct temporal patterns of immune modulation were also observed. Using
408 flow cytometry, TAC and PRED induced minimal effects on cellular composition (**Figure**
409 **4D**), and MMF selectively reduced CD4+ T cells by day 30 (**Figure 4A, D**). FTY showed
410 the most dynamic changes, increasing B220+ B cells while decreasing CD4+ T cells at
411 day 7 (**Figure 4B, D**), followed by elevated Foxp3+ Tregs and decreased CD4+ T cells
412 by day 30 (**Figure 4C, D**). IHC analysis revealed complementary changes in cellular
413 distribution and stromal architecture. TAC showed transient effects, characterized by
414 increased Treg distribution in the CR at day 7 (**Figure 4E, I, Supplemental Figure 7A**)
415 without affecting laminin ratios (**Figure 4G-J, Supplemental Figure 7C, D**). PRED
416 demonstrated only early structural changes, marked by increased La4:La5 at day 3
417 **(Figure 4E-J, Supplemental Figure 7A-D)**. MMF showed the most consistent pro-
418 tolerogenic profile, maintaining increased Treg distribution throughout the treatment
419 period **(Figure 4E, F, I, J, Supplemental Figure 7A, B)** and a higher La4:La5 at day 3
420 **(Figure 4G-J, Supplemental Figure 7C, D)**. FTY showed early pro-tolerogenic effects
421 with increased Treg distribution and La4:La5 at day 3, but not at later time points
422 **(Figure 4E-J, Supplemental Figure 7A-D)**. Together, these findings demonstrated that
423 all four immunosuppressants, particularly MMF and FTY, predominantly promoted a
424 pro-tolerogenic state in pLNs, characterized by increased Tregs and/or elevated laminin
425 α4:α5 ratios particularly during early treatment phases. This contrasted with the pro-

426 inflammatory environment observed in mLNs, suggesting differential regulation of
427 immune organization between loco-regional and systemic lymphoid tissue
428 compartments.

429 MMF and FTY counteract alloantigen-induced pro-inflammatory changes through dual
430 regulation of Tregs and LN architecture

431 Given the pronounced effects of MMF and FTY on LN organization under homeostatic
432 conditions (**Figure 3H, I, 4I, J**), we next utilized a mouse model with allogeneic
433 stimulation (Allo) to assess their impact on transplant-related alloimmune responses,
434 mimicking the immunologic stress of solid organ transplantation. Mice were injected with
435 fully allogeneic splenocytes ($10^7$ cells intravenously) followed by MMF or FTY
436 administration for 3 days. Compared to the no treatment controls, Allo alone did not
437 affect Treg distribution in mLNs or pLNs (**Figure 5A, C**). However, when combined with
438 either drug, significant increases in Tregs were observed. Compared to Allo alone, MMF
439 increased Tregs around mLN HEV, and FTY increased Tregs in both mLN HEV and
440 pLN HEV and CR (**Figure 5A, C, E, F**). Allo alone decreased La4:La5 in both pLN and
441 mLN (**Figure 5B, D**), indicating a pro-inflammatory shift caused by alloantigen-induced
442 immune responses, consistent with our previous findings [15]. When combined with MMF
443 or FTY, both drugs prevented this decrease, maintaining laminin α4:α5 ratios
444 comparable to untreated controls **(Figure 5B, D, E, F)**. These findings demonstrated
445 that MMF and FTY inhibited alloantigen-induced pro-inflammatory shifts in LN through
446 two complementary mechanisms: increasing Tregs and preserving tolerogenic laminin
447 stromal architecture. This dual action suggested that these drugs may be particularly
448 effective at promoting a tolerogenic environment during allogeneic immune challenges.

449 MMF and FTY effects are mediated through FRC-derived laminins α4 and α5

450 Given the significant impact of MMF and FTY on LN architecture, particularly through
451 modulation of La4:La5 under both homeostatic and allogeneic stimulated conditions, we
452 next investigated whether these drugs directly influenced FRC-derived laminins, given
453 the crucial role of FRC in modulating laminin expression [14,20]. We utilized two laminin
454 KO mouse strains: FRC-Laminin4-KO mice (Pdgfrb-Cre+/- × La4$^{fl/fl}$) have the laminin α4
455 gene specifically deleted in FRCs, and FRC-Laminin5-KO mice (Pdgfrb-Cre+/- × La5$^{fl/fl}$)
456 have the laminin α5 gene specifically deleted in FRCs [14,52]. FRC-Lama4-KO and FRC-
457 Lama5-KO mice were treated with MMF or FTY for 3 days, to specifically examine
458 whether FRC-derived laminin α4 and α5 played a role in immunosuppressant-mediated
459 effects on LN stromal organization.
460
461 In mLNs, as we observed in WT mice, 3-day treatment of MMF or FTY did not affect
462 laminin ratios (**Figure 3F-I, Supplemental Figure 6C, D**). In FRC-Lama4-KO mice,
463 MMF and FTY also did not affect laminin ratios (**Figure 6A-C, M**). However, in FRC-
464 Lama5-KO mice, both drugs decreased the La4:La5 in CR of mLNs (**Figure 6D-F, M**).
465 These results suggested that MMF and FTY effects on laminin composition were
466 dependent on the FRC-derived laminin expression, indicating its critical role in
467 maintaining the laminin balance in the mLN. The removal of FRC-derived laminin α5
468 appeared to unmask an early pro-inflammatory impact of MMF and FTY that was
469 otherwise absent. This indicated that laminins specifically from FRCs acted as a
470 protective factor in preserving stromal homeostasis in the mLNs, counteracting the early
471 disruptive effects of these immunosuppressants.

472

473 In pLNs, as we observed in WT mice, 3-day treatment of WT mice with MMF or FTY
474 each increased La4:La5 (**Figure 4G-J, Supplemental Figure 7C, D**). MMF also
475 increased La4:La5 in both CR and HEV of FRC-Lama5-KO mice (**Figure 6J-L, N**), but
476 not in FRC-Lama4-KO mice (**Figure 6J-L, N**). In contrast, FTY decreased La4:La5 in
477 CR of FRC-Lama4-KO mice (**Figure 6G-I, N**) but not in FRC-Lama5-KO mice (**Figure**
478 **6J-L, N**). These findings indicated that MMF and FTY modulated La4:La5 through
479 distinct mechanisms that depended on the presence of laminins α4 and α5 from FRCs,
480 although the precise pathways involved remain to be determined. The analysis of these
481 KO models revealed that MMF relied on laminin α4 to increase laminin ratios, as its
482 absence in FRC-Lama4-KO mice abolished the increase in La4:La5, while laminin α5
483 deficiency did not. Conversely, FTY depended on laminin α5 to maintain the La4:La5
484 ratio, as its absence revealed a decrease. These results demonstrated the distinct roles
485 of laminins α4 and α5 in mediating immunosuppressant effects by remodeling LN
486 architecture under MMF or FTY treatment. Collectively, these findings suggested a
487 broader mechanistic link between immunosuppressive drugs and immune regulation,
488 extending beyond their direct cellular effects to include the critical role of FRC-derived
489 laminins in maintaining LN homeostasis

490 **Discussion**

491 The gut plays as a critical role in maintaining transplant tolerance by serving as a key
492 interface between the immune system and environmental stimuli [53-55]. In this study, we
493 performed an in-depth characterization of the previously underappreciated, complex
494 interplay of immunosuppressants and several gut-associated processes, including the
495 microbiome and metabolism, intestinal gene expression, mesenteric and peripheral LN
496 organization, and lymphocyte trafficking over time. Though not designed to target the
497 gut, our findings revealed that immunosuppressants exert profound, time-dependent
498 effects on the gut environment. While early treatment exhibits distinct, drug-specific
499 effects, prolonged immunosuppressant use leads to a convergent dysbiotic state in the
500 gut microbiome by day 30. A particularly striking observation is the convergent
501 enrichment of the *Muribaculaceae* family across all four drugs after long-term treatment.
502 These bacteria harbor a repertoire of enzymes capable of efficiently breaking down
503 complex carbohydrates and proteins [42-44], providing them with a competitive edge in an
504 altered gut environment under immune suppression. Their metabolic versatility likely
505 enables them to thrive under conditions of disrupted gut homeostasis, implying that
506 sustained immunosuppression selectively favors organisms adapted to such changes.
507 Furthermore, recent work identifying *Muribaculaceae* as pathobionts capable of
508 inducing diabetes [45] offer a potential mechanistic link between prolonged
509 immunosuppression and the metabolic complications often seen in transplant patients
510 [56-58]. This suggests that extended immune suppression may trigger a common
511 mechanism affecting microbial communities.
512

513 Immune suppressants also triggered a common mechanism affecting epithelial and
514 mucosal immunity (illustrated in **Figure 7**). All immunosuppressants disrupt antigen-
515 driven B cell activation. Previous studies reported glucocorticoids directly suppress B
516 cell function by inhibiting NF-κB-dependent transcription, leading to reduced expression
517 of cytokines, costimulatory molecules, and survival factors essential for B cell activation
518 and differentiation [59,60]. Calcineurin inhibitors impair NFAT-dependent signaling by
519 blocking dephosphorylation of NFAT proteins, thereby inhibiting transcriptional
520 programs involved in B cell proliferation and antibody production while also inhibiting
521 helper T cells [61]. In contrast, mTOR inhibitors and anti-metabolites interfere more
522 indirectly by suppressing T follicular helper (Tfh) cell development and function, leading
523 to impaired T cell-dependent B cell help, germinal center formation, and class-switch
524 recombination [62]. While mucosal adaptive immunity is predominately suppressed, the
525 upregulation of a class-switched mechanism, as in Ighg2b gene activation, suggests
526 selective survival or expansion of mucosal-associated or microbiota-reactive B cell
527 subsets. This is supported by epithelial gene expression patterns, showing early
528 induction of circadian resetting program and xenobiotic detoxification pathways,
529 followed by late activation of antimicrobial peptides, ROS-generating oxidases, and
530 stress-responsive enzymes. These changes point to a compensatory host mechanism
531 to counteract potential pathobiont expansion and epithelial stress. However, prolonged
532 treatments still led to transcriptomic changes in epithelial regenerative capacity, lipid
533 metabolism, and structural remodeling. These impaired intestinal functions may
534 predispose the mucosa to vulnerability during sustained immunosuppressive therapy.
535 Overall, these findings reveal a complex interplay between immunosuppressive drug

536 disturbance and the host's attempt to preserve mucosal homeostasis. Further
537 experiments to pinpoint the precise intestinal responders common to all immune
538 suppressants classes will be essential to understand off-target drug effects and to guide
539 strategies to mitigate complications.
540
541 Beyond shared microbial and intestinal shifts, each immunosuppressant exhibited
542 distinct intestinal and metabolic signatures that revealed both intended and unintended
543 mechanistic insights. By day 30, intestinal gene expression profiles became increasingly
544 broad, underscoring the tissue's heightened susceptibility to off-target drug effects.
545 These differences likely arise from a combination of direct pharmacologic actions on
546 host epithelial and immune cells, compensatory host responses, and complex
547 interactions with the gut microbiota. At the metabolic level, each drug elicited shared
548 and unique luminal metabolomic changes. TAC broadly altered amino acid metabolism
549 and reduced levels of microbial-derived metabolites such as SCFAs, consistent with its
550 known gastrointestinal side effects such as diarrhea and nonspecific abdominal
551 discomfort [63]. PRED exerted a widespread suppressive effect on metabolism, consistent
552 with its ability to inhibit cellular functions and pro-inflammatory cytokines [64]. This
553 resulting reduction in amino acid derivatives, SCFAs, TMA, and polyamines provides
554 insights into its side effects, including diabetes and osteoporosis [47-49]. MMF targeted
555 purine metabolism via IMPDH inhibition and suppressed the TCA cycle and branched-
556 chain amino acid (BCAA) pathways, impairing ATP production and enterocyte protein
557 synthesis. This may underlie its distinct profile of gastrointestinal toxicity and
558 inflammation [65,66], compromised barrier integrity [36], and increased epithelial apoptosis

559 and villous atrophy [67]. FTY, in contrast, produced the mildest metabolic disruption,
560 primarily affecting nucleotide turnover and polyamine biosynthesis, a profile that may
561 explain its generally better tolerability [68].
562
563 Despite their distinct profiles, all immunosuppressants consistently affected amino acid
564 metabolism and energy processing, suggesting a fundamental mechanism underlying
565 long-term immunosuppression. The reduction in SCFA-producing bacteria can disrupt
566 metabolic processes such as blood pressure regulation, lipogenesis, and blood glucose
567 control [69]. Studies have demonstrated that probiotics can reverse conditions like
568 tacrolimus-induced gut dysbiosis, MMF-related intestinal toxicity and inflammation,
569 SCFA depletion, and hypertension by restoring the vascular redox state and improving
570 endothelial nitric oxide synthase (eNOS) function [69-72]. On the other hand, differences in
571 how these drugs alter amino acid metabolism indicate that each exerts distinct
572 influences on protein synthesis and cellular energy balance, which may explain their
573 varying effects on different immune cell populations. Arginine metabolism, for example,
574 is critical because it affects eNOS activity through the arginine-NO pathway, influencing
575 NO production and ROS generation, changes that can impair endothelial function and
576 modulate immune cell activation [73]. Both calcineurin and mTOR inhibitors drastically
577 affect amino acid regulation [31], including arginine metabolism, which aligns with their
578 documented vascular complications [74-76] and supports targeted probiotic therapies to
579 mitigate adverse metabolic and vascular outcomes. Ultimately, the shared and drug-
580 specific intestinal and metabolic signatures represent actionable targets for monitoring

581 and mitigating off-target toxicity, offering new opportunities to improve safety and
582 precision in transplantation medicine.
583
584 The impact of immunosuppressants on lymphoid tissue organization further illustrates
585 the complex nature of their effects. Our data revealed anatomically distinct and
586 temporally dynamic responses with lymphoid tissues. pLNs maintained an anti-
587 inflammatory state, evidenced by elevated Tregs and increased La4:La5 ratios,
588 particularly during early treatment phases. This response is consistent with the intended
589 immunosuppressive action of these drugs. In contrast, mLNs, which drain the intestine,
590 eventually developed a pro-inflammatory environment, characterized by reduced Tregs
591 and decreased La4:La5. This compartment-specific regulatory effect may underlie some
592 of the gastrointestinal side effects observed with immunosuppression [32]. As illustrated in
593 **Figure 7**, these changes likely reflect feedback from the intestinal microenvironment,
594 where metabolic stress and mucosal adaptation shape lymphoid architecture. Further
595 insights into LN FRC-derived laminins α4 and α5 in mediating these effects suggest that
596 stromal responses play a key role in mediating these effects [14]. Notably, MMF and FTY
597 both preserved tolerogenic LN architecture during allostimulation through the dual
598 regulation of Tregs and stromal organization, though they were distinctly dependent on
599 laminin α4 or laminin α5. These findings highlight a critical gap in our understanding of
600 how immunosuppressive drugs precisely affect the gene expression, function, and
601 phenotype of LNSCs, and they emphasize the need for further research to develop
602 more precise therapeutic strategies.
603

604 This study does have several limitations. Our 30-day mouse studies may not fully
605 capture the complexity of long-term immunosuppression in human transplant patients,
606 and extended longitudinal studies are needed to better mirror clinical outcomes.
607 Moreover, we evaluated single drugs rather than the combination regimens commonly
608 used in clinical practice. Additionally, although our allogeneic stimulation model
609 provided valuable insights into transplant-related alloimmune responses, the absence of
610 an allograft precluded the pro-inflammatory context typical of solid organ
611 transplantation, potentially underestimating the drug impact on immune regulation
612 during active alloimmune responses. Nonetheless, our study established fundamental
613 insights into immunosuppressants effects, and revealed an underappreciated while
614 profound impacts on the intestine microenvironment, providing a critical basis for future
615 transplant investigations. Overall, our findings highlight an understudied aspect of
616 immunosuppressant effects on the intestine and lymphoid tissue, emphasizing the need
617 for strategies such as conserved biomarker-monitoring, microbiome-targeted
618 interventions, and tissue-specific drug delivery to enhance therapeutic precision and
619 reduce side effects.

620 **Methods and Materials**

621 Study approval

622 All procedures, as described previously [31,32,77,78] involving mice were performed in
623 accordance with the guidelines and regulations set by the Office of Animal Welfare
624 Assurance of the University of Maryland School of Medicine under the approved IACUC
625 protocol nos. 05150001, 0318002, 1220001, and AUP-00000397.

626 Reagents

627 USP grade immunosuppressants were used, when available. All drugs were prepared in
628 a manner approved by the University of Maryland School of Medicine IACUC: TAC
629 (USP grade, MilliporeSigma, Burlington, MA) was reconstituted in DMSO (USP grade,
630 MilliporeSigma) at 20 mg/ml for storage. At time of use, TAC/DMSO stock was diluted
631 with absolute ethanol (USP grade, Decon Labs, King of Prussia, PA) to 1.5 mg/ml then
632 further diluted 1:5 in sterile PBS and injected at 10 µl/gm s.c. (3 mg/kg/day) [30]. PRED
633 (MilliporeSigma) was reconstituted in PBS at 50 mg/ml for storage and then diluted to
634 0.5 mg/ml in PBS and injected at 5mg/kg/d i.p. [79]. MMF (MilliporeSigma) was
635 reconstituted at 30 mg/ml in DMSO for storage and then diluted in PBS to 1.5 mg/ml
636 and at 30 mg/kg/d i.p. [80]. FTY (Fingolimod, MilliporeSigma) was reconstituted at 3
637 mg/ml in 1:1 PBS:Ethanol for storage and then diluted 1:10 in PBS and administered at
638 3 mg/kg/d p.o.[81]. The control group received PBS only.

639 Mice experiments

640 Mouse experiments were performed according to ARRIVE guidelines
641 (https://arriveguidelines.org). 8- to 14-week-old female C57BL/6 mice were purchased

642 from The Jackson Laboratory (Bar Harbor, ME, USA). Mice were maintained at the
643 University of Maryland School of Medicine Veterinary Resources animal facility. Only
644 female mice were used to ensure a high degree of homogeneity within our study
645 groups. The Pdgfrb-Cre+/– x La4fl/fl [52] and Pdgfrb-Cre+/– x La5fl/fl [14] conditional
646 knockout (KO) mice were previously developed in our laboratory. All mice were
647 cohoused for a minimum of 2 weeks prior to experiments to normalize microbiota.
648 During this period, mice from different treatment groups were housed in the same room
649 and adjacent cages under identical conditions to ensure normalized environmental
650 exposure. At experimental day 0, the mice were randomly separated to different
651 experimental groups, and then kept groups in separate cages to prevent cross
652 exposure. Mice received daily immunosuppression following the dosages in **Table 2**. In
653 allogeneic stimulation experiment, mice received 10^7 fully allogeneic BALB/c
654 splenocytes intravenously (i.v.) on day 0 followed by drug treatment. On the day of
655 harvest, the mice were euthanized by $CO_2$ narcosis, intraluminal stool samples collected
656 for metabolomic and microbiome analyses, cardiac puncture utilized for blood collection,
657 and mesenteric and peripheral (axillary, inguinal, and brachial) LNs and portions of the
658 small intestine between the duodenum and jejunum harvested for immunological
659 assays. All procedures involving mice were performed in accordance with the guidelines
660 and regulations set by the Office of Animal Welfare Assurance of the University of
661 Maryland School of Medicine.

662 <u>Stool specimen collection, DNA extraction, and metagenomic sequencing</u>

663 As described previously [31,32,77,78], stool samples were collected and stored immediately in
664 DNA/RNA Shields (Zymo Research, Irvine, CA, USA) at -80°C. This stabilizes and

665 protects the integrity of nucleic acids and minimizes the need for immediate processing
666 of specimens. The Quick-DNA Fecal/Soil Microbe kit (Zymo Research, Irvine, CA, USA)
667 was used to extract DNA from 0.15-0.25 grams of fecal samples. To ensure that no
668 exogenous DNA contaminated the samples, we included negative extraction controls.
669 Construction of the metagenomic sequencing libraries was performed as previously
670 [31,32,78]. In brief, the Nextera XT Flex Kit (Illumina), according to the manufacturer's
671 recommendations, libraries were then pooled together in equimolar proportions before
672 they were sequenced on a single Illumina NovaSeq 6000 S2 flow cell at Maryland
673 Genomics at the University of Maryland School of Medicine. 92.7±8.5 (mean±s.e.) million
674 reads per sample were obtained.

675 Gut microbiome analyses

676 Sequence analyses were performed as previously described [31,32,77,78]. Metagenomic
677 sequence reads mapping to Genome Reference Consortium Mouse Build 39 of strain
678 C57BL/6J (GRCm39) were removed using BMTagger v3.101 [82]. Sequence read pairs
679 were removed when one or both the read pairs matched the genome reference. The
680 Illumina adapter was trimmed and quality assessment was performed using default
681 parameters in fastp (v.0.21.0) [83]. The taxonomic composition of the microbiomes was
682 established using Kraken2 (v.2020.12) and Braken (v. 2.5.0) using the comprehensive
683 mouse microbiota genome catalog [84]. Phyloseq R package (v1.38.0) was used to
684 generate the barplot and diversity index. Linear discriminant analysis (LDA) effect size
685 (LEfSe) analysis was used to identify fecal phylotypes that could explain the differences.
686 The α value for the non-parametric factorial Kruskal-Wallis (KW) sum-rank test was set
687 at 0.05 and the threshold for the logarithmic LDA model score for discriminative features

688 was set at 2.0. An all-against-all BLAST search was performed in the multiclass
689 analysis. Taxonomic ordination graphs were created with the microViz (v0.12.4) [85]. The
690 metagenomic dataset was mapped to the protein database UniRef90 to ensure the
691 comprehensive coverage in functional annotation, and was then summarized using
692 HUMAnN3 (Human Microbiome Project Unified Metabolic Analysis Network) (v0.11.2)
693 to determine the presence, absence, and abundance of metabolic pathways in a
694 microbial community. MetaCyc pathway definitions and MinPath were used to identify a
695 parsimonious set of pathways summarized in HUMAnN3 in the microbial community.
696 Canonical Correspondence Analysis (CCA) was performed using the vegan package
697 [86,87] based on the Bray-Curtis distance. Based on their eigenvalues, CA1 and CA2 were
698 selected as the major components. To evaluate microbiome profile differences across
699 groups and time points, the line plot was generated using the average pairwise Bray-
700 Curtis distances between all group pairs at each time point.

701 Metabolite extraction and metabolome analyses

702 As previously described [31,32,77,78], capillary electrophoresis-mass spectrometry (CE/MS)
703 was used for measuring metabolome of intraluminal stool (luminal/local) to obtain a
704 comprehensive quantitative survey of metabolites (Human Metabolome Technologies,
705 Boston, MA, USA) for immunosuppressants TAC, PRED, MMF, and a no-treatment
706 control group processed concurrently. For FTY, stool pellets were collected at the same
707 time points for metabolomic analysis due to technical limitations in obtaining sufficient
708 sample volumes for comprehensive profiling. The no-treatment control for FTY also
709 used stool pellets and processed concurrently. All subsequent analyses were performed
710 using the respective no-treatment control groups and the same specimen types,

711 processed concurrently with their corresponding experimental groups, to ensure valid
712 comparisons. ~10-30 mg of stool was weighed at the time of collection using a
713 company-provided vial and stored at -80°C until shipped to vendor on dry ice. QC
714 procedures included standards, sample blanks and internal controls that were evenly
715 spaced among the samples analyzed. Compound identification was performed using a
716 CE/MS library of >1,600 annotated molecules.
717
718 To reduce the influence of measurement noise, rigorous data pretreatment was
719 performed according to validated procedures [88] and are as previously described [31,32,78].
720 Metabolites were annotated using PubChem [89], KEGG [90], and HMDB [91] annotation
721 frameworks that leverage cataloged chemical compounds, known metabolic
722 characterization, and functional hierarchy (i.e., reaction, modules, pathways). Partial
723 least squares discriminant analysis (PLS-DA) implemented using mixOmics (vers.
724 6.18.1) was used [92]. The "sparseness" of the model was adjusted by the number of
725 components in the model and the number of variables within each component based on
726 the classification error rate with respect to the number of selected variables. Tuning was
727 performed one component at a time, and the optimal number of variables to select was
728 calculated. The volcano plot combines results from fold change (FC) analysis to show
729 significantly increased metabolites after 7-day tacrolimus treatment. A metabolite is
730 shown if FC is >2 and the p-value is <0.05 based on 2-sample t-tests. Original
731 metabolite measurements without normalization were used in the FC analysis. For the
732 metabolites annotated in a specific functional pathway, metabolite set enrichment
733 analysis (MSEA) was performed [93].

734 RNA isolation, transcriptome sequencing, and bioinformatics analyses

735 RNA isolation, transcriptome sequencing, and bioinformatics analyses are as previously
736 described [31,32,78]. Dissected intestinal tissues were stored immediately in RNAlater
737 solution (QIAGEN) in RNAse-free tubes (Denville Scientific, Holliston, MA) to stabilize
738 and protect the integrity of RNA [94]. Specimens were stored at −80°C until extraction.
739 For each sample, total RNA was extracted from ~1 cm of ileum. Prior to the extraction,
740 500 µl of ice-cold RNase free PBS was added to the sample. To remove the RNAlater,
741 the mixture was centrifuged at 8,000x*g* for 10 min and the resulting pellet resuspended
742 in 500 µl ice-cold RNase-free PBS with 10 µl of β-mercaptoethanol. A tissue suspension
743 was obtained by bead beating procedure using the FastPrep lysing matrix B protocol
744 (MP Biomedicals, Solon, OH) to homogenized tissues. RNA was extracted from the
745 resulting suspension using TRIzol Reagent (Invitrogen, Carlsbad, CA) following the
746 manufacturer's recommendations and followed by protein cleanup using Phasemaker
747 tubes (Invitrogen) and precipitation of total nucleic acids using isopropanol. RNA was
748 resuspended in DEPC-treated DNAase/RNAase-free water. Residual DNA was purged
749 from total RNA extract by treating once with TURBO DNase (Ambion, Austin, TX, Cat.
750 No. AM1907) according to the manufacturer's protocol. DNA removal was confirmed via
751 PCR assay using 16S rRNA primer 27 F (5′-AGAGTTTGATCCTGGCTCAG-3′) and
752 534 R (5′-CATTACCGCGGCTGCTGG-3′). The quality of extracted RNA was verified
753 using the Agilent 2100 Expert Bioanalyzer using the RNA 1000 Nano kit (Agilent
754 Technologies, Santa Clara, CA). Ribosomal RNA depletion and library construction
755 were performed using the RiboZero Plus kit and TruSeq stranded mRNA library
756 preparation kit (Illumina) according to the manufacturer's recommendations. Libraries

757 were then pooled together in equimolar proportions and sequenced on a single Illumina
758 NovaSeq 6000 S2 flow cell at the Genomic Resource Center (Institute for Genome
759 Sciences, University of Maryland School of Medicine) using the 150 bp paired-end
760 protocol. 143,2±53.4 (mean±s.e.) million reads per sample were obtained. The quality of
761 sequencing was evaluated by using FastQC [95]. Reads were aligned to the mouse
762 genome (Mus_musculus.GRCm39) using HiSat (version HISAT2-2.0.4) [96] and the
763 number of reads that aligned to the coding regions was determined using HTSeq [97].
764 Significant differential expression was assessed using DESeq2 [98] with an FDR value ≤
765 0.05 and FC>2. The over-representative analysis was done by importing Differentially
766 Expressed Genes (DEGs) against GO ontologies using the enrichGO function of
767 clusterProfile Bioconductor package [99]. Only the ontology terms with q value <0.05 were
768 used for plotting. The normalized enrichment score was calculated as the ratio of the
769 proportion of DEGs annotated to a given GO term to the proportion of genes in the
770 reference annotated to the same GO term. UpSet plots were generated using UpSetR
771 (vers. 1.4.0) to analyze overlapping DEGs between days 7 and 30 and across different
772 treatments.

773 Flow cytometry

774 The procedure is as previously described [31,32]. To produce single-cell suspensions, LNs
775 were disaggregated and passed through 70-μm nylon mesh screens (Thermo Fisher
776 Scientific, Waltham, MA). Antibodies against surface molecules were incubated with cell
777 suspensions for 30 min at 4°C (**Supplemental Table 4**) then washed with FACS buffer
778 [PBS with 0.5% w/v bovine serum albumin] twice. Cells were then permeabilized,
779 according to manufacturer's protocol, with Foxp3/Transcription Factor Staining Buffer

780 Set (eBioscience, San Diego, CA), washed with FACS buffer, and subsequently stained
781 with antibodies for intracellular molecules at 4°C. Samples were analyzed with an LSR
782 Fortessa Cell Analyzer (BD Biosciences), and data were analyzed using FlowJo
783 software version 10.6 (BD Biosciences). Single color controls (cells stained with single
784 surface marker antibody) and unstained controls were used for flow channel
785 compensation.

786 Immunohistochemistry

787 We excised mLN, pLN and segments of the intestine between the duodenum and jejunum
788 then immediately submerged in OCT compound (Scigen Paramount, CA, USA).
789 Cryosections (6-7 μm for LNs, 10 μm for intestine) were cut in duplicate or triplicate
790 depending on size of block using a Microm HM 550 cryostat (ThermoFisher Scientific).
791 Slides were then fixed in cold 1:1 acetone:methanol for 5 min, air dried for 15 min, and
792 stored at -80°C until use. At the time of staining, slides were thawed for 15 minutes at
793 room temperature then sections were rehydrated in PBS and blocked with 10%
794 secondary antibody host serum PBST (PBS + 0.03% Triton-X-100 + 0.5% BSA). The
795 slides were then stained for 1 hour with primary antibodies at room temperature (diluted
796 1:50-1:200 in PBST) for 1 hour incubated with secondary antibodies (diluted 1:100-1:400
797 in PBST) for 1 hour. After staining, slides were fixed with 4% paraformaldehyde in PBS
798 for 5 min, quenched with 1% glycerol in PBS for 5 min, and mounted with Prolong Gold
799 Antifade Mountant with or without DAPI (Thermo Fisher Scientific). Images were acquired
800 using Accu-Scope EXC-500/Nikon (Accu-Scope, Commack, NY, and Nikon, Tokyo,
801 Japan) and analyzed using Volocity software (Quorum Technologies Inc., Sacramento,
802 CA). The antibodies used are listed in **Supplemental Table 4**. For each mouse, 1-2 mLNs

803 and 2-3 pLNs, and 1 piece of intestine were collected. All samples from each treatment
804 group were combined and analyzed as a block, 2-3 sections/block were placed on slides,
805 and 7-30 fields/slide were analyzed. The average of MFI for each treatment group was
806 calculated by averaging the MFI values across all slides from all mice, within demarcated
807 HEVs and CR regions of mLN and pLN and whole intestinal images. Qualitative heat
808 maps were generated (GraphPad prism) to express changes in IHC marker expression
809 level relative to control using -1 to represent “decreased” (blue in the heatmap), 0 to
810 represent “unchanged” (white in the heatmap), and 1 to represent “increased” (red in the
811 heatmap). GraphPad Prism 10.3.1 (San Diego, CA, USA) was used for analysis with
812 statistical significance defined as $P < 0.05$. Tukey’s multiple comparison tests of one-way
813 ANOVA were used for comparisons of fluorescence.
814

## Declarations

### Ethics Approval and Consent to Participate

All experimental procedures involving mice were approved by and performed in accordance with the guidelines and regulations of the Institutional Animal Care and Use Committee (IACUC) of the University of Maryland School of Medicine under the approved protocol numbers 05150001, 0318002, 1220001, and AUP-0000397.

### Consent for Publication

Not applicable.

### Availability of data and materials

The authors confirm that the data supporting the findings of this study are available within the article and indicated supplementary materials. The data that support the findings of this study are openly available; metagenome sequences were submitted to GenBank under BioProject PRJNA809764 (https://www.ncbi.nlm.nih.gov/bioproject/PRJNA809764) with the SRA study ID SRP361281. RNA-Seq data were deposited in the NCBI Gene Expression Omnibus database (GSE288074). The preprint of this study is available at https://doi.org/10.1101/2025.01.02.631100.

### Competing interests

No potential financial and non-financial conflict of interest was reported by the authors.

### Funding Declaration

This work was supported by the National Institute of Health (NIH) National Heart, Lung and Blood Institute award R01HL148672 (JSB/BM), NIH National Institute of Allergy and

Infectious Diseases U01AI170050 (BM/JSB/VM), R01AI114496 (JSB) and training grant T32AI95190-10 (SJG). University of Maryland Baltimore ORD-OTT No. BM-2025-077.

**Authors' contributions**

B. M., L. W., and J. S. B. designed the experiments. L. W., A. K., S. J. G., D. K., L. L., R. L., V. S., W. P., M. W., and B. L. conducted and analyzed the mice experiments. H. W. L. performed nucleic acid extraction and sequencing library preparation. B. M. and Y. S. performed the bioinformatics analyses. B. M., L. W., A. K., S. J. G., M. F., Y. S., and J. S. B. wrote the manuscript. B. M. and J. S. B. are co-corresponding authors for this manuscript.

846 **References**


847 1. Lodhi, S.A., Lamb, K.E., and Meier-Kriesche, H.U. (2011). Solid Organ Allograft Survival
848 Improvement in the United States: The Long-Term Does Not Mirror the Dramatic Short-
849 Term Success. American Journal of Transplantation *11*, 1226-1235. 10.1111/j.1600-
850 6143.2011.03539.x.
851 2. Dai, H., Zheng, Y., Thomson, A.W., and Rogers, N.M. (2020). Transplant Tolerance
852 Induction: Insights From the Liver. Frontiers in Immunology *11*.
853 10.3389/fimmu.2020.01044.
854 3. Fishman, J.A. (2017). Infection in Organ Transplantation. Am J Transplant *17*, 856-879.
855 10.1111/ajt.14208.
856 4. Gallagher, M.P., Kelly, P.J., Jardine, M., Perkovic, V., Cass, A., Craig, J.C., Eris, J., and
857 Webster, A.C. (2010). Long-term cancer risk of immunosuppressive regimens after
858 kidney transplantation. J Am Soc Nephrol *21*, 852-858. 10.1681/ASN.2009101043.
859 5. Schmitz, V., Klawitter, J., Bendrick-Peart, J., Schoening, W., Puhl, G., Haschke, M.,
860 Klawitter, J., Consoer, J., Rivard, C.J., Chan, L., et al. (2009). Metabolic profiles in urine
861 reflect nephrotoxicity of sirolimus and cyclosporine following rat kidney transplantation.
862 Nephron Exp Nephrol *111*, e80-91. 10.1159/000209208.
863 6. Gioco, R., Corona, D., Ekser, B., Puzzo, L., Inserra, G., Pinto, F., Schipa, C., Privitera, F.,
864 Veroux, P., and Veroux, M. (2020). Gastrointestinal complications after kidney
865 transplantation. World J Gastroenterol *26*, 5797-5811. 10.3748/wjg.v26.i38.5797.
866 7. Wijdicks, E.F. (2001). Neurotoxicity of immunosuppressive drugs. Liver Transpl *7*, 937-
867 942. 10.1053/jlts.2001.27475.
868 8. Bhat, M., Usmani, S.E., Azhie, A., and Woo, M. (2021). Metabolic Consequences of Solid
869 Organ Transplantation. Endocr Rev *42*, 171-197. 10.1210/endrev/bnaa030.
870 9. Nayak, S.P., Bagchi, B., and Roy, S. (2022). Effects of immunosuppressants on T-cell
871 dynamics: Understanding from a generic coarse-grained immune network model. J
872 Biosci *47*. 10.1007/s12038-022-00312-4.
873 10. Xie, H., Zhu, H., Zhou, K., Wan, J., Zhang, L., Yang, Z., Zhou, L., Chen, X., Xu, X., Zheng, S.,
874 and Wang, H. (2020). Target-oriented delivery of self-assembled immunosuppressant
875 cocktails prolongs allogeneic orthotopic liver transplant survival. J Control Release *328*,
876 237-250. 10.1016/j.jconrel.2020.08.043.
877 11. Saxena, V., Li, L., Paluskievicz, C., Kasinath, V., Bean, A., Abdi, R., Jewell, C.M., and
878 Bromberg, J.S. (2019). Role of lymph node stroma and microenvironment in T cell
879 tolerance. Immunol Rev *292*, 9-23. 10.1111/imr.12799.
880 12. Li, L., Wu, J., Abdi, R., Jewell, C.M., and Bromberg, J.S. (2021). Lymph node fibroblastic
881 reticular cells steer immune responses. Trends Immunol *42*, 723-734.
882 10.1016/j.it.2021.06.006.
883 13. Mueller, S.N., Hosiawa-Meagher, K.A., Konieczny, B.T., Sullivan, B.M., Bachmann, M.F.,
884 Locksley, R.M., Ahmed, R., and Matloubian, M. (2007). Regulation of homeostatic
885 chemokine expression and cell trafficking during immune responses. Science *317*, 670-
886 674. 10.1126/science.1144830.

887 14. Li, L., Shirkey, M.W., Zhang, T., Xiong, Y., Piao, W., Saxena, V., Paluskievicz, C., Lee, Y.,
888 Toney, N., Cerel, B.M., et al. (2020). The lymph node stromal laminin alpha5 shapes
889 alloimmunity. J Clin Invest *130*, 2602-2619. 10.1172/JCI135099.
890 15. Simon, T., Li, L., Wagner, C., Zhang, T., Saxena, V., Brinkman, C.C., Tostanoski, L.H.,
891 Ostrand-Rosenberg, S., Jewell, C., Shea-Donohue, T., et al. (2019). Differential
892 Regulation of T-cell Immunity and Tolerance by Stromal Laminin Expressed in the Lymph
893 Node. Transplantation *103*, 2075-2089. 10.1097/TP.0000000000002774.
894 16. Maarouf, O.H., Uehara, M., Kasinath, V., Solhjou, Z., Banouni, N., Bahmani, B., Jiang, L.,
895 Yilmam, O.A., Guleria, I., Lovitch, S.B., et al. (2018). Repetitive ischemic injuries to the
896 kidneys result in lymph node fibrosis and impaired healing. JCI Insight *3*.
897 10.1172/jci.insight.120546.
898 17. Mongodin, E.F., Saxena, V., Iyyathurai, J., Lakhan, R., Ma, B., Silverman, E., Lee, Z.L., and
899 Bromberg, J.S. (2021). Chronic rejection as a persisting phantom menace in organ
900 transplantation: a new hope in the microbiota? Curr Opin Organ Transplant *26*, 567-581.
901 10.1097/MOT.0000000000000929.
902 18. Scott, E.N., Gocher, A.M., Workman, C.J., and Vignali, D.A.A. (2021). Regulatory T Cells:
903 Barriers of Immune Infiltration Into the Tumor Microenvironment. Front Immunol *12*,
904 702726. 10.3389/fimmu.2021.702726.
905 19. Lu, J., Li, P., Du, X., Liu, Y., Zhang, B., and Qi, F. (2021). Regulatory T cells induce
906 transplant immune tolerance. Transpl Immunol *67*, 101411.
907 10.1016/j.trim.2021.101411.
908 20. Warren, K.J., Iwami, D., Harris, D.G., Bromberg, J.S., and Burrell, B.E. (2014). Laminins
909 affect T cell trafficking and allograft fate. J Clin Invest *124*, 2204-2218.
910 10.1172/JCI73683.
911 21. Anggelia, M.R., Cheng, H.Y., Chuang, W.Y., Hsieh, Y.H., Wang, A.Y.L., Lin, C.H., Wei, F.C.,
912 Brandacher, G., and Lin, C.H. (2021). Unraveling the Crucial Roles of FoxP3+ Regulatory T
913 Cells in Vascularized Composite Allograft Tolerance Induction and Maintenance.
914 Transplantation *105*, 1238-1249. 10.1097/TP.0000000000003509.
915 22. Lei, Y.M., Chen, L., Wang, Y., Stefka, A.T., Molinero, L.L., Theriault, B., Aquino-Michaels,
916 K., Sivan, A.S., Nagler, C.R., Gajewski, T.F., et al. (2016). The composition of the
917 microbiota modulates allograft rejection. J Clin Invest *126*, 2736-2744.
918 10.1172/JCI85295.
919 23. Hossain, M.S., Jaye, D.L., Pollack, B.P., Farris, A.B., Tselanyane, M.L., David, E., Roback,
920 J.D., Gewirtz, A.T., and Waller, E.K. (2011). Flagellin, a TLR5 agonist, reduces graft-
921 versus-host disease in allogeneic hematopoietic stem cell transplantation recipients
922 while enhancing antiviral immunity. J Immunol *187*, 5130-5140.
923 10.4049/jimmunol.1101334.
924 24. Jenq, R.R., Ubeda, C., Taur, Y., Menezes, C.C., Khanin, R., Dudakov, J.A., Liu, C., West,
925 M.L., Singer, N.V., Equinda, M.J., et al. (2012). Regulation of intestinal inflammation by
926 microbiota following allogeneic bone marrow transplantation. J Exp Med *209*, 903-911.
927 10.1084/jem.20112408.
928 25. Oh, P.L., Martinez, I., Sun, Y., Walter, J., Peterson, D.A., and Mercer, D.F. (2012).
929 Characterization of the ileal microbiota in rejecting and nonrejecting recipients of small
930 bowel transplants. Am J Transplant *12*, 753-762. 10.1111/j.1600-6143.2011.03860.x.

931 26. Willner, D.L., Hugenholtz, P., Yerkovich, S.T., Tan, M.E., Daly, J.N., Lachner, N., Hopkins,
932 P.M., and Chambers, D.C. (2013). Reestablishment of recipient-associated microbiota in
933 the lung allograft is linked to reduced risk of bronchiolitis obliterans syndrome. Am J
934 Respir Crit Care Med *187*, 640-647. 10.1164/rccm.201209-1680OC.
935 27. Kensiski, A., Gavzy, S.J., Wu, L., Mas, V., Ma, B., and Bromberg, J.S. (2025).
936 Immunosuppressant imprecision: multidirectional effects on metabolism and
937 microbiome. Clin Microbiol Rev, e0017824. 10.1128/cmr.00178-24.
938 28. Koren, O., Goodrich, J.K., Cullender, T.C., Spor, A., Laitinen, K., Backhed, H.K., Gonzalez,
939 A., Werner, J.J., Angenent, L.T., Knight, R., et al. (2012). Host remodeling of the gut
940 microbiome and metabolic changes during pregnancy. Cell *150*, 470-480.
941 10.1016/j.cell.2012.07.008.
942 29. Rooks, M.G., Veiga, P., Wardwell-Scott, L.H., Tickle, T., Segata, N., Michaud, M., Gallini,
943 C.A., Beal, C., van Hylckama-Vlieg, J.E., Ballal, S.A., et al. (2014). Gut microbiome
944 composition and function in experimental colitis during active disease and treatment-
945 induced remission. The ISME journal *8*, 1403-1417. 10.1038/ismej.2014.3.
946 30. Bromberg, J.S., Hittle, L., Xiong, Y., Saxena, V., Smyth, E.M., Li, L., Zhang, T., Wagner, C.,
947 Fricke, W.F., Simon, T., et al. (2018). Gut microbiota-dependent modulation of innate
948 immunity and lymph node remodeling affects cardiac allograft outcomes. JCI Insight *3*.
949 10.1172/jci.insight.121045.
950 31. Wu, L., Kensiski, A., Gavzy, S.J., Lwin, H.W., Song, Y., France, M.T., Lakhan, R., Kong, D.,
951 Li, L., Saxena, V., et al. (2025). Rapamycin immunomodulation utilizes time-dependent
952 alterations of lymph node architecture, leukocyte trafficking, and gut microbiome. JCI
953 Insight *10*. 10.1172/jci.insight.186505.
954 32. Ma, B., Gavzy, S.J., France, M., Song, Y., Lwin, H.W., Kensiski, A., Saxena, V., Piao, W.,
955 Lakhan, R., Iyyathurai, J., et al. (2023). Rapid intestinal and systemic metabolic
956 reprogramming in an immunosuppressed environment. BMC Microbiol *23*, 394.
957 10.1186/s12866-023-03141-z.
958 33. Gao, Y., and Tian, T. (2023). mTOR Signaling Pathway and Gut Microbiota in Various
959 Disorders: Mechanisms and Potential Drugs in Pharmacotherapy. Int J Mol Sci *24*.
960 10.3390/ijms241411811.
961 34. Liu, Y., Yang, F., Zou, S., and Qu, L. (2018). Rapamycin: A Bacteria-Derived
962 Immunosuppressant That Has Anti-atherosclerotic Effects and Its Clinical Application.
963 Front Pharmacol *9*, 1520. 10.3389/fphar.2018.01520.
964 35. Nayak, R.R., Alexander, M., Deshpande, I., Stapleton-Gray, K., Rimal, B., Patterson, A.D.,
965 Ubeda, C., Scher, J.U., and Turnbaugh, P.J. (2021). Methotrexate impacts conserved
966 pathways in diverse human gut bacteria leading to decreased host immune activation.
967 Cell Host Microbe *29*, 362-377 e311. 10.1016/j.chom.2020.12.008.
968 36. Khan, N., Binder, L., Pantakani, D.V.K., and Asif, A.R. (2017). MPA Modulates Tight
969 Junctions' Permeability via Midkine/PI3K Pathway in Caco-2 Cells: A Possible Mechanism
970 of Leak-Flux Diarrhea in Organ Transplanted Patients. Frontiers in physiology *8*, 438.
971 10.3389/fphys.2017.00438.
972 37. Wilson, I.D., and Nicholson, J.K. (2017). Gut microbiome interactions with drug
973 metabolism, efficacy, and toxicity. Transl Res *179*, 204-222. 10.1016/j.trsl.2016.08.002.

974 38. Haiser, H.J., Gootenberg, D.B., Chatman, K., Sirasani, G., Balskus, E.P., and Turnbaugh,
975 P.J. (2013). Predicting and manipulating cardiac drug inactivation by the human gut
976 bacterium Eggerthella lenta. Science *341*, 295-298. 10.1126/science.1235872.
977 39. Taylor, M.R., Flannigan, K.L., Rahim, H., Mohamud, A., Lewis, I.A., Hirota, S.A., and
978 Greenway, S.C. (2019). Vancomycin relieves mycophenolate mofetil-induced
979 gastrointestinal toxicity by eliminating gut bacterial beta-glucuronidase activity. Sci Adv
980 *5*, eaax2358. 10.1126/sciadv.aax2358.
981 40. Kieser, S., Zdobnov, E.M., and Trajkovski, M. (2021). Comprehensive mouse gut
982 metagenome catalog reveals major difference to the human counterpart. bioRxiv,
983 2021.2003.2018.435958. 10.1101/2021.03.18.435958.
984 41. Franzosa, E.A., McIver, L.J., Rahnavard, G., Thompson, L.R., Schirmer, M., Weingart, G.,
985 Lipson, K.S., Knight, R., Caporaso, J.G., Segata, N., and Huttenhower, C. (2018). Species-
986 level functional profiling of metagenomes and metatranscriptomes. Nat Methods *15*,
987 962-968. 10.1038/s41592-018-0176-y.
988 42. Ormerod, K.L., Wood, D.L., Lachner, N., Gellatly, S.L., Daly, J.N., Parsons, J.D., Dal'Molin,
989 C.G., Palfreyman, R.W., Nielsen, L.K., Cooper, M.A., et al. (2016). Genomic
990 characterization of the uncultured Bacteroidales family S24-7 inhabiting the guts of
991 homeothermic animals. Microbiome *4*, 36. 10.1186/s40168-016-0181-2.
992 43. Lagkouvardos, I., Lesker, T.R., Hitch, T.C.A., Galvez, E.J.C., Smit, N., Neuhaus, K., Wang, J.,
993 Baines, J.F., Abt, B., Stecher, B., et al. (2019). Sequence and cultivation study of
994 Muribaculaceae reveals novel species, host preference, and functional potential of this
995 yet undescribed family. Microbiome *7*, 28. 10.1186/s40168-019-0637-2.
996 44. Smith, B.J., Miller, R.A., and Schmidt, T.M. (2021). Muribaculaceae Genomes Assembled
997 from Metagenomes Suggest Genetic Drivers of Differential Response to Acarbose
998 Treatment in Mice. mSphere *6*, e0085121. 10.1128/msphere.00851-21.
999 45. Yang, X., Wang, Z., Niu, J., Zhai, R., Xue, X., Wu, G., Fang, Y., Meng, G., Yuan, H., Zhao, L.,
1000 and Zhang, C. (2023). Pathobionts from chemically disrupted gut microbiota induce
1001 insulin-dependent diabetes in mice. Microbiome *11*, 62. 10.1186/s40168-023-01507-z.
1002 46. Bevins, C.L., and Salzman, N.H. (2011). Paneth cells, antimicrobial peptides and
1003 maintenance of intestinal homeostasis. Nat Rev Microbiol *9*, 356-368.
1004 10.1038/nrmicro2546.
1005 47. van Raalte, D.H., Ouwens, D.M., and Diamant, M. (2009). Novel insights into
1006 glucocorticoid-mediated diabetogenic effects: towards expansion of therapeutic
1007 options? Eur J Clin Invest *39*, 81-93. 10.1111/j.1365-2362.2008.02067.x.
1008 48. Compston, J. (2018). Glucocorticoid-induced osteoporosis: an update. Endocrine *61*, 7-
1009 16. 10.1007/s12020-018-1588-2.
1010 49. Eastell, R., Reid, D.M., Compston, J., Cooper, C., Fogelman, I., Francis, R.M., Hosking,
1011 D.J., Purdie, D.W., Ralston, S.H., Reeve, J., et al. (1998). A UK Consensus Group on
1012 management of glucocorticoid-induced osteoporosis: an update. J Intern Med *244*, 271-
1013 292. 10.1046/j.1365-2796.1998.00408.x.
1014 50. Sintchak, M.D., Fleming, M.A., Futer, O., Raybuck, S.A., Chambers, S.P., Caron, P.R.,
1015 Murcko, M.A., and Wilson, K.P. (1996). Structure and mechanism of inosine
1016 monophosphate dehydrogenase in complex with the immunosuppressant mycophenolic
1017 acid. Cell *85*, 921-930. 10.1016/s0092-8674(00)81275-1.

1018 51. Heischmann, S., Dzieciatkowska, M., Hansen, K., Leibfritz, D., and Christians, U. (2017).
1019 The Immunosuppressant Mycophenolic Acid Alters Nucleotide and Lipid Metabolism in
1020 an Intestinal Cell Model. Sci Rep *7*, 45088. 10.1038/srep45088.
1021 52. Li, L., Shirkey, M.W., Zhang, T., Piao, W., Li, X., Zhao, J., Mei, Z., Guo, Y., Saxena, V.,
1022 Kensiski, A., et al. (2022). Lymph node fibroblastic reticular cells preserve a tolerogenic
1023 niche in allograft transplantation through laminin alpha4. J Clin Invest *132*.
1024 10.1172/JCI156994.
1025 53. Honda, K., and Littman, D.R. (2016). The microbiota in adaptive immune homeostasis
1026 and disease. Nature *535*, 75-84. 10.1038/nature18848.
1027 54. Gabarre, P., Loens, C., Tamzali, Y., Barrou, B., Jaisser, F., and Tourret, J. (2022).
1028 Immunosuppressive therapy after solid organ transplantation and the gut microbiota:
1029 Bidirectional interactions with clinical consequences. Am J Transplant *22*, 1014-1030.
1030 10.1111/ajt.16836.
1031 55. Salvadori, M., and Rosso, G. (2024). Update on the reciprocal interference between
1032 immunosuppressive therapy and gut microbiota after kidney transplantation. World J
1033 Transplant *14*, 90194. 10.5500/wjt.v14.i1.90194.
1034 56. Kato, T., Chan, M.C., Gao, S.Z., Schroeder, J.S., Yokota, M., Murohara, T., Iwase, M.,
1035 Noda, A., Hunt, S.A., and Valantine, H.A. (2004). Glucose intolerance, as reflected by
1036 hemoglobin A1c level, is associated with the incidence and severity of transplant
1037 coronary artery disease. J Am Coll Cardiol *43*, 1034-1041. 10.1016/j.jacc.2003.08.063.
1038 57. Valantine, H., Rickenbacker, P., Kemna, M., Hunt, S., Chen, Y.D., Reaven, G., and Stinson,
1039 E.B. (2001). Metabolic abnormalities characteristic of dysmetabolic syndrome predict
1040 the development of transplant coronary artery disease: a prospective study. Circulation
1041 *103*, 2144-2152. 10.1161/01.cir.103.17.2144.
1042 58. Biadi, O., Potena, L., Fearon, W.F., Luikart, H.I., Yeung, A., Ferrara, R., Hunt, S.A.,
1043 Mocarski, E.S., and Valantine, H.A. (2007). Interplay between systemic inflammation and
1044 markers of insulin resistance in cardiovascular prognosis after heart transplantation. J
1045 Heart Lung Transplant *26*, 324-330. 10.1016/j.healun.2007.01.020.
1046 59. Ashwell, J.D., Lu, F.W., and Vacchio, M.S. (2000). Glucocorticoids in T cell development
1047 and function*. Annu Rev Immunol *18*, 309-345. 10.1146/annurev.immunol.18.1.309.
1048 60. Franchimont, D. (2004). Overview of the actions of glucocorticoids on the immune
1049 response: a good model to characterize new pathways of immunosuppression for new
1050 treatment strategies. Ann N Y Acad Sci *1024*, 124-137. 10.1196/annals.1321.009.
1051 61. Macian, F., Lopez-Rodriguez, C., and Rao, A. (2001). Partners in transcription: NFAT and
1052 AP-1. Oncogene *20*, 2476-2489. 10.1038/sj.onc.1204386.
1053 62. Araki, K., Turner, A.P., Shaffer, V.O., Gangappa, S., Keller, S.A., Bachmann, M.F., Larsen,
1054 C.P., and Ahmed, R. (2009). mTOR regulates memory CD8 T-cell differentiation. Nature
1055 *460*, 108-112. 10.1038/nature08155.
1056 63. Scott, L.J., McKeage, K., Keam, S.J., and Plosker, G.L. (2003). Tacrolimus: a further update
1057 of its use in the management of organ transplantation. Drugs *63*, 1247-1297.
1058 10.2165/00003495-200363120-00006.
1059 64. Rhen, T., and Cidlowski, J.A. (2005). Antiinflammatory action of glucocorticoids--new
1060 mechanisms for old drugs. N Engl J Med *353*, 1711-1723. 10.1056/NEJMra050541.

1061 65. Shipkova, M., Armstrong, V.W., Oellerich, M., and Wieland, E. (2003). Acyl glucuronide
1062 drug metabolites: toxicological and analytical implications. Ther Drug Monit *25*, 1-16.
1063 10.1097/00007691-200302000-00001.
1064 66. Oellerich, M., Shipkova, M., Schutz, E., Wieland, E., Weber, L., Tonshoff, B., and
1065 Armstrong, V.W. (2000). Pharmacokinetic and metabolic investigations of mycophenolic
1066 acid in pediatric patients after renal transplantation: implications for therapeutic drug
1067 monitoring. German Study Group on Mycophenolate Mofetil Therapy in Pediatric Renal
1068 Transplant Recipients. Ther Drug Monit *22*, 20-26. 10.1097/00007691-200002000-
1069 00004.
1070 67. Helderman, J.H., and Goral, S. (2002). Gastrointestinal complications of transplant
1071 immunosuppression. J Am Soc Nephrol *13*, 277-287. 10.1681/ASN.V131277.
1072 68. Tedesco-Silva, H., Mourad, G., Kahan, B.D., Boira, J.G., Weimar, W., Mulgaonkar, S.,
1073 Nashan, B., Madsen, S., Charpentier, B., Pellet, P., and Vanrenterghem, Y. (2005).
1074 FTY720, a novel immunomodulator: efficacy and safety results from the first phase 2A
1075 study in de novo renal transplantation. Transplantation *79*, 1553-1560.
1076 69. Bhat, M., Pasini, E., Copeland, J., Angeli, M., Husain, S., Kumar, D., Renner, E., Teterina,
1077 A., Allard, J., Guttman, D.S., and Humar, A. (2017). Impact of Immunosuppression on the
1078 Metagenomic Composition of the Intestinal Microbiome: a Systems Biology Approach to
1079 Post-Transplant Diabetes. Sci Rep *7*, 10277. 10.1038/s41598-017-10471-2.
1080 70. Toral, M., Romero, M., Rodriguez-Nogales, A., Jimenez, R., Robles-Vera, I., Algieri, F.,
1081 Chueca-Porcuna, N., Sanchez, M., de la Visitacion, N., Olivares, M., et al. (2018).
1082 Lactobacillus fermentum Improves Tacrolimus-Induced Hypertension by Restoring
1083 Vascular Redox State and Improving eNOS Coupling. Mol Nutr Food Res *62*, e1800033.
1084 10.1002/mnfr.201800033.
1085 71. Robles-Vera, I., Toral, M., de la Visitacion, N., Sanchez, M., Gomez-Guzman, M., Romero,
1086 M., Yang, T., Izquierdo-Garcia, J.L., Jimenez, R., Ruiz-Cabello, J., et al. (2020). Probiotics
1087 Prevent Dysbiosis and the Rise in Blood Pressure in Genetic Hypertension: Role of Short-
1088 Chain Fatty Acids. Mol Nutr Food Res *64*, e1900616. 10.1002/mnfr.201900616.
1089 72. Jardou, M., Provost, Q., Brossier, C., Pinault, E., Sauvage, F.L., and Lawson, R. (2021).
1090 Alteration of the gut microbiome in mycophenolate-induced enteropathy: impacts on
1091 the profile of short-chain fatty acids in a mouse model. BMC Pharmacol Toxicol *22*, 66.
1092 10.1186/s40360-021-00536-4.
1093 73. Fleissner, F., and Thum, T. (2011). Critical role of the nitric oxide/reactive oxygen species
1094 balance in endothelial progenitor dysfunction. Antioxid Redox Signal *15*, 933-948.
1095 10.1089/ars.2010.3502.
1096 74. Wang, S., Lu, J., You, Q., Huang, H., Chen, Y., and Liu, K. (2016). The mTOR/AP-1/VEGF
1097 signaling pathway regulates vascular endothelial cell growth. Oncotarget *7*, 53269-
1098 53276. 10.18632/oncotarget.10756.
1099 75. Wang, Y., Li, Q., Zhang, Z., Peng, K., Zhang, D.M., Yang, Q., Passerini, A.G., Simon, S.I.,
1100 and Sun, C. (2022). mTOR contributes to endothelium-dependent vasorelaxation by
1101 promoting eNOS expression and preventing eNOS uncoupling. Commun Biol *5*, 726.
1102 10.1038/s42003-022-03653-w.
1103 76. Rodrigues-Diez, R., Gonzalez-Guerrero, C., Ocana-Salceda, C., Rodrigues-Diez, R.R.,
1104 Egido, J., Ortiz, A., Ruiz-Ortega, M., and Ramos, A.M. (2016). Calcineurin inhibitors

1105 cyclosporine A and tacrolimus induce vascular inflammation and endothelial activation
1106 through TLR4 signaling. Sci Rep *6*, 27915. 10.1038/srep27915.
1107 77. Bromberg, J.S., Hittle, L.E., Xiong, Y., Saxena, V., Smyth, E.M., Li, L., Zhang, T., Wagner,
1108 C., Fricke, W.F., Simon, T., et al. (2018). Gut microbiota–dependent modulation of innate
1109 immunity and lymph node remodeling affects cardiac allograft outcomes. JCI Insight *3*.
1110 10.1172/jci. insight.121045.
1111 78. Ma, B., Gavzy, S.J., Saxena, V., Song, Y., Piao, W., Lwin, H.W., Lakhan, R., Iyyathurai, J., Li,
1112 L., France, M., et al. (2023). Strain-specific alterations in gut microbiome and host
1113 immune responses elicited by tolerogenic Bifidobacterium pseudolongum. Sci Rep *13*,
1114 1023. 10.1038/s41598-023-27706-0.
1115 79. Chin, H.J., Chae, D.W., Kim, Y.C., An, W.S., Ihm, C., Jin, D.C., Kim, S.G., Kim, Y.L., Kim, Y.S.,
1116 Kim, Y.G., et al. (2021). Comparison of the Efficacy and Safety of Tacrolimus and Low-
1117 Dose Corticosteroid with High-Dose Corticosteroid for Minimal Change Nephrotic
1118 Syndrome in Adults. J Am Soc Nephrol *32*, 199-210. 10.1681/ASN.2019050546.
1119 80. Richez, C., Richards, R.J., Duffau, P., Weitzner, Z., Andry, C.D., Rifkin, I.R., and
1120 Aprahamian, T. (2013). The effect of mycophenolate mofetil on disease development in
1121 the gld.apoE (-/-) mouse model of accelerated atherosclerosis and systemic lupus
1122 erythematosus. PLoS One *8*, e61042. 10.1371/journal.pone.0061042.
1123 81. Honig, S.M., Fu, S., Mao, X., Yopp, A., Gunn, M.D., Randolph, G.J., and Bromberg, J.S.
1124 (2003). FTY720 stimulates multidrug transporter– and cysteinyl leukotriene–dependent
1125 T cell chemotaxis to lymph nodes. Journal of Clinical Investigation *111*, 627-637.
1126 10.1172/jci200316200.
1127 82. Rotmistrovsky, K., and Agarwala, R., B. (2011). BMTagger: Best Match Tagger for
1128 removing human reads from metagenomics datasets (Integrative Human Microbiome
1129 Project (iHMP) by NCBI/NLM, National Institutes of Health).
1130 83. Chen, S., Zhou, Y., Chen, Y., and Gu, J. (2018). fastp: an ultra-fast all-in-one FASTQ
1131 preprocessor. Bioinformatics *34*, i884-i890. 10.1093/bioinformatics/bty560.
1132 84. Kieser, S., Zdobnov, E.M., and Trajkovski, M. (2022). Comprehensive mouse microbiota
1133 genome catalog reveals major difference to its human counterpart. PLoS Comput Biol
1134 *18*, e1009947. 10.1371/journal.pcbi.1009947.
1135 85. D.J., B., I.C. Arts, and Penders, J. (2021). microViz: an R package for microbiome data
1136 visualization and statistics. J Open Source Softw *6*, 3201.
1137 https://doi.org/10.21105/joss.03201.
1138 86. Jari Oksanen, F.G.B., Michael Friendly, Roeland Kindt, Pierre Legendre, Dan McGlinn,
1139 Peter R. Minchin, R. B. O'Hara, Gavin L. Simpson, Peter Solymos, M. Henry H. Stevens,
1140 Eduard Szoecs and Helene Wagner (2016). vegan: Community Ecology Package. R
1141 package.
1142 87. Dixon, P. (2003). VEGAN, a package of R functions for community ecology. Journal of
1143 Vegetation Science *14*, 927-930.
1144 88. van den Berg, R.A., Hoefsloot, H.C., Westerhuis, J.A., Smilde, A.K., and van der Werf, M.J.
1145 (2006). Centering, scaling, and transformations: improving the biological information
1146 content of metabolomics data. BMC Genomics *7*, 142. 10.1186/1471-2164-7-142.

1147 89. Kim, S., Chen, J., Cheng, T., Gindulyte, A., He, J., He, S., Li, Q., Shoemaker, B.A., Thiessen,
1148 P.A., Yu, B., et al. (2021). PubChem in 2021: new data content and improved web
1149 interfaces. Nucleic Acids Res *49*, D1388-D1395. 10.1093/nar/gkaa971.
1150 90. Hattori, M., Tanaka, N., Kanehisa, M., and Goto, S. (2010). SIMCOMP/SUBCOMP:
1151 chemical structure search servers for network analyses. Nucleic Acids Res *38*, W652-656.
1152 10.1093/nar/gkq367.
1153 91. Wishart, D.S., Feunang, Y.D., Marcu, A., Guo, A.C., Liang, K., Vazquez-Fresno, R., Sajed,
1154 T., Johnson, D., Li, C., Karu, N., et al. (2018). HMDB 4.0: the human metabolome
1155 database for 2018. Nucleic Acids Res *46*, D608-D617. 10.1093/nar/gkx1089.
1156 92. Le Cao, K.A., Boitard, S., and Besse, P. (2011). Sparse PLS discriminant analysis:
1157 biologically relevant feature selection and graphical displays for multiclass problems.
1158 BMC Bioinformatics *12*, 253. 10.1186/1471-2105-12-253.
1159 93. Xia, J., and Wishart, D.S. (2010). MSEA: a web-based tool to identify biologically
1160 meaningful patterns in quantitative metabolomic data. Nucleic Acids Res *38*, W71-77.
1161 10.1093/nar/gkq329.
1162 94. Gorokhova, E. (2005). Effects of preservation and storage of microcrustaceans in
1163 RNAlater on RNA and DNA degradation. . Limnol. Oceanogr.: Methods *3*, 143–148.
1164 95. Andrews, S. (2010). FastQC: A Quality Control Tool for High Throughput Sequence Data.
1165 Available online at: http://www.bioinformatics.babraham.ac.uk/projects/fastqc/.
1166 96. Kim, D., Langmead, B., and Salzberg, S.L. (2015). HISAT: a fast spliced aligner with low
1167 memory requirements. Nat Methods *12*, 357-360. 10.1038/nmeth.3317.
1168 97. Anders, S., Pyl, P.T., and Huber, W. (2015). HTSeq--a Python framework to work with
1169 high-throughput sequencing data. Bioinformatics *31*, 166-169.
1170 10.1093/bioinformatics/btu638.
1171 98. Anders, S., and Huber, W. (2010). Differential expression analysis for sequence count
1172 data. Genome Biol *11*, R106. 10.1186/gb-2010-11-10-r106.
1173 99. G. Yu, L. Wang, Y. Han, and He, Q. (2012). clusterProfiler: an R package for comparing
1174 biological themes among gene clusters. OMICS: A Journal of Integrative Biology *16*, 284-
1175 287. 10.1089/omi.2011.0118.
1176 100. Bromberg, J.S., Hittle, L., Xiong, Y., Saxena, V., Smyth, E.M., Li, L., Zhang, T., Wagner, C.,
1177 Fricke, W.F., Simon, T., et al. (2018). Gut microbiota–dependent modulation of innate
1178 immunity and lymph node remodeling affects cardiac allograft outcomes. JCI Insight *3*.
1179 10.1172/jci.insight.121045.
1180 101. Beeton, C., Richez, C., Richards, R.J., Duffau, P., Weitzner, Z., Andry, C.D., Rifkin, I.R., and
1181 Aprahamian, T. (2013). The Effect of Mycophenolate Mofetil on Disease Development in
1182 the gld.apoE−/− Mouse Model of Accelerated Atherosclerosis and Systemic Lupus
1183 Erythematosus. PLoS ONE *8*, e61042. 10.1371/journal.pone.0061042.
1184 102. Honig, S.M., Fu, S., Mao, X., Yopp, A., Gunn, M.D., Randolph, G.J., and Bromberg, J.S.
1185 (2003). FTY720 stimulates multidrug transporter- and cysteinyl leukotriene-dependent T
1186 cell chemotaxis to lymph nodes. Journal of Clinical Investigation *111*, 627-637.
1187 10.1172/JCI200316200.
1188

1189 **Tables**

1190 **Table 1**. Differential metabolite abundance in gut lumen after 7 days of

1191 immunosuppressant treatment *

| | TAC | PRED | MMF | FTY |
|---|---|---|---|---|
| ↑ | **31**<br>• Amino acids & derivatives<br>• Pyrimidine metabolism<br>• Sugars and sugar phosphates | **4** | **4** | **14**<br>• Purine metabolism<br>• Arginine metabolism |
| ↓ | **28**<br>• Polyamines & derivatives<br>• SCFAs, TMA | **95**<br>• Amino acids & derivatives<br>• SCFAs, TMA<br>• Pyrimidine metabolism<br>• Polyamines & derivatives | **37**<br>• Glyoxylate and Dicarboxylate<br>• Branched-chain amino acids & derivatives<br>• Purine metabolism<br>• Neurotransmitters | **22**<br>• Pyrimidine metabolism<br>• SCFAs |
| *subtotal* | **59** | **99** | **41** | **36** |

1192 * Gut luminal metabolites with significant changes (fold change >2, $p<0.05$) after 7 days of
1193 treatment with tacrolimus (TAC), prednisone (PRED), mycophenolate mofetil (MMF), or
1194 Fingolimod (FTY) compared to untreated controls. Numbers in bold indicate total metabolites
1195 significantly increased (↑) or decreased (↓) for each drug. Key metabolic pathways affected are
1196 listed for each drug. SCFAs: short-chain fatty acids; TMA: trimethylamine. Data derived from
1197 untargeted metabolomics analysis using capillary electrophoresis-mass spectrometry.

1198 **Table 2.** Immunosuppression drugs and dosage.

| Treatment Groups | Dose*(mg/kg/day) | Source (catalog #) | Route |
|---|---|---|---|
| **Tacrolimus** | 3 mg/kg/day | Sigma Aldrich (Y0001926) | Subcutaneous [100] |
| **Prednisolone** | 5 mg/kg/day | Sigma Aldrich (P6004) | Intraperitoneal [79] |
| **Mycophenolate mofetil** | 30 mg/kg/day | Sigma Aldrich (SML0284) | Intraperitoneal [101] |
| **FTY** | 3 mg/kg/day | Sigma Aldrich **(**SML0700**)** | Oral [102] |

1199

1200 **Figure legends**

1201 **Figure 1: Impact of immunosuppressant treatment on gut microbiome**
1202 **composition and function.** Pairwise Bray-Curtis distance analysis comparing drug-
1203 treated groups to untreated controls and between different treatment groups to measure
1204 changes in **A)** taxonomic composition, and **B)** functional pathway abundance. Distances
1205 represent mean values per group. Untreated mice as control group. **C**) Principal
1206 Components Analysis of gut microbiome composition based on Bray-Curtis distance.
1207 Robust centered log ratio transformation applied on count compositional data. **D)**
1208 Differentially abundant taxonomic groups identified by pairwise comparisons between
1209 treatment groups and controls. Changes in abundance are expressed as log2 fold
1210 changes relative to control group.

1211

1212 **Figure 2: Immunosuppressants temporally shift intestinal immune responses. A**)
1213 Bar plots showing the number of differentially expressed genes (DEGs) after 7 and 30
1214 days of treatment compared to the control group. Yellow and blue bars indicate the
1215 number of upregulated genes, while red and green bars represent the number of
1216 downregulated genes. **B**) Heatmap DEGs in intestinal tissue following treatment with
1217 five immunosuppressant drugs at days 7 and 30. Transcriptomic data from rapamycin-
1218 treated mice from our previously study [31] integrated in current analysis. Genes defined
1219 as differentially expressed in at least four of the five drug treatment groups at either time
1220 point. Hierarchical clustering performed on both genes (rows) and samples (columns)
1221 using Euclidean distance and ward linkage. Color scale indicates normalized Z-scores
1222 of expression values, with red denoting upregulation and blue denoting downregulation

1223 relative to no-treatment controls. **C**) Functional enrichment analysis of conserved
1224 intestinal transcriptional responses to immunosuppressant treatments. Dot plot showing
1225 over-represented Gene Ontology (GO) biological process pathway based on DEGs at
1226 days 7 and 30. EnrichGO pathways containing more than three genes were included in
1227 this plot. Dot size denotes the normalized enrichment score. Blue downregulated and
1228 red upregulated pathways; color shaded based on the $-\log_{10}$(p-value) of enrichment.
1229 **Abbr**: TAC: tacrolimus, MMF: mycophenolate mofetil, PRED: prednisone, FTY:
1230 fingolimod, RAPA: rapamycin
1231
1232 **Figure 3: Effects of TAC, PRED, MMF, and FTY on mLN cell content, cell**
1233 **distribution, and structure.** Flow cytometry analysis of **A)** B220+ B cells and CD4+ T
1234 cells on day 30 after PRED treatment and **B)** Foxp3+ Tregs on day 30 after FTY
1235 treatment in mLNs. **C)** Heatmaps depict changes in expression with TAC, PRED, MMF,
1236 and FTY relative to controls in mLNs after 3, 7, and 30 days of treatment. IHC of **D)** CR
1237 and **E)** HEV Foxp3+ Tregs on days 3, 7, and 30 in mLNs. IHC of **F)** CR and **G)** HEV
1238 La4: La5 on days 3, 7, and 30 in mLNs. Barplot showing detailed plots at each timepoint
1239 are in **Supplemental Figure 6.** Heatmaps depict changes in expression with TAC,
1240 PRED, MMF, and FTY relative to controls in **H)** CR and **I)** around HEV in mLNs. 3
1241 mice/group. 2-3 LNs/mouse, 2-3 sections/LN, 7-30 fields/tissue. One-way ANOVA. * $p <$
1242 $0.05$; ** $p < 0.01$, *** $p < 0.001$, **** $p < 0.0001$.
1243
1244 **Figure 4: Effects of TAC, PRED, MMF, and FTY on pLN cell content, cell**
1245 **distribution, and structure.** Flow cytometry analysis of **A)** CD4+ T cells on day 30

1246 after MMF treatment, and **B)** B220+ B cells and CD4+ T cells on day 7 and **C)** CD4+ T
1247 cells and Foxp3+ Tregs after FTY treatment in pLNs. **D)** Heatmaps depict changes in
1248 expression with TAC, PRED, MMF, and FTY relative to controls in pLNs after 3, 7, and
1249 30 days of treatment. IHC of **E)** CR and **F)** HEV Foxp3+ Tregs on days 3, 7, and 30 in
1250 pLNs. IHC of **G)** CR and **H)** La4: La5 on days 3, 7, and 30 in pLNs. Barplot showing
1251 detailed plots at each timepoint are in **Supplemental Figure 7.** Heatmaps depict
1252 changes in expression with TAC, PRED, MMF, and FTY relative to controls in **I)** CR and
1253 **J)** around HEV in pLNs. 3 mice/group. 2-3 LNs/mouse, 2-3 sections/LN, 7-30
1254 fields/tissue. One-way ANOVA. * $p < 0.05$; ** $p < 0.01$, *** $p < 0.001$, **** $p < 0.0001$.
1255
1256 **Figure 5. MMF and FTY induce a rapid anti-inflammatory response during**
1257 **allogeneic stimulation.** IHC for Foxp3+ Tregs in the **A**) pLN and **C**) mLN. La4:La5 in
1258 **B**) pLN and **D**) mLN. Heatmap summarizes significant changes in expression
1259 comparing allogeneic stimulation plus MMF or FTY to allogeneic stimulation alone in **E**)
1260 pLNs and **F**) mLNs. 3 mice/group. 2-3 LNs/mouse, 2-3 sections/LN, 7-30 fields/tissue.
1261 One-way ANOVA: * $p < 0.05$, ** $p < 0.01$, *** $p < 0.001$, **** $p < 0.0001$.
1262
1263 **Figure 6. MMF and FTY decrease the La4:La5 in FRC-Lama5-KO mLNs and pLNs.**
1264 IHC showing **A, D, G, J**) laminin α4; **B, E, H, K**) laminin α5; and **C, F, I, L**) La4:La5 in
1265 mLNs **(A-F, M)** and pLNs **(G-L, N)** of WT and FRC-Lama4-KO (**A-C and G-I**) and FRC-
1266 Lama5-KO mice (**D-F and J-L**) on day 3. **M, N**) Heatmap summarizes significant
1267 changes relative to controls in **M)** mLN and **N)** pLN. 3-5 mice/group. 2-3 LNs/mouse, 2-

1268 3 sections/LN, 7-30 fields/tissue. One-way ANOVA: * $p < 0.05$, ** $p < 0.01$, *** $p <$

1269 $0.001$, **** $p < 0.0001$.

1270

1271 **Figure 7**. Illustration of shared intestinal responses in response to immunosuppressant

1272 regimens. Created in BioRender. Ma, B. (2025) https://BioRender.com/ctcfgx9.

1273 **Figure 1.**

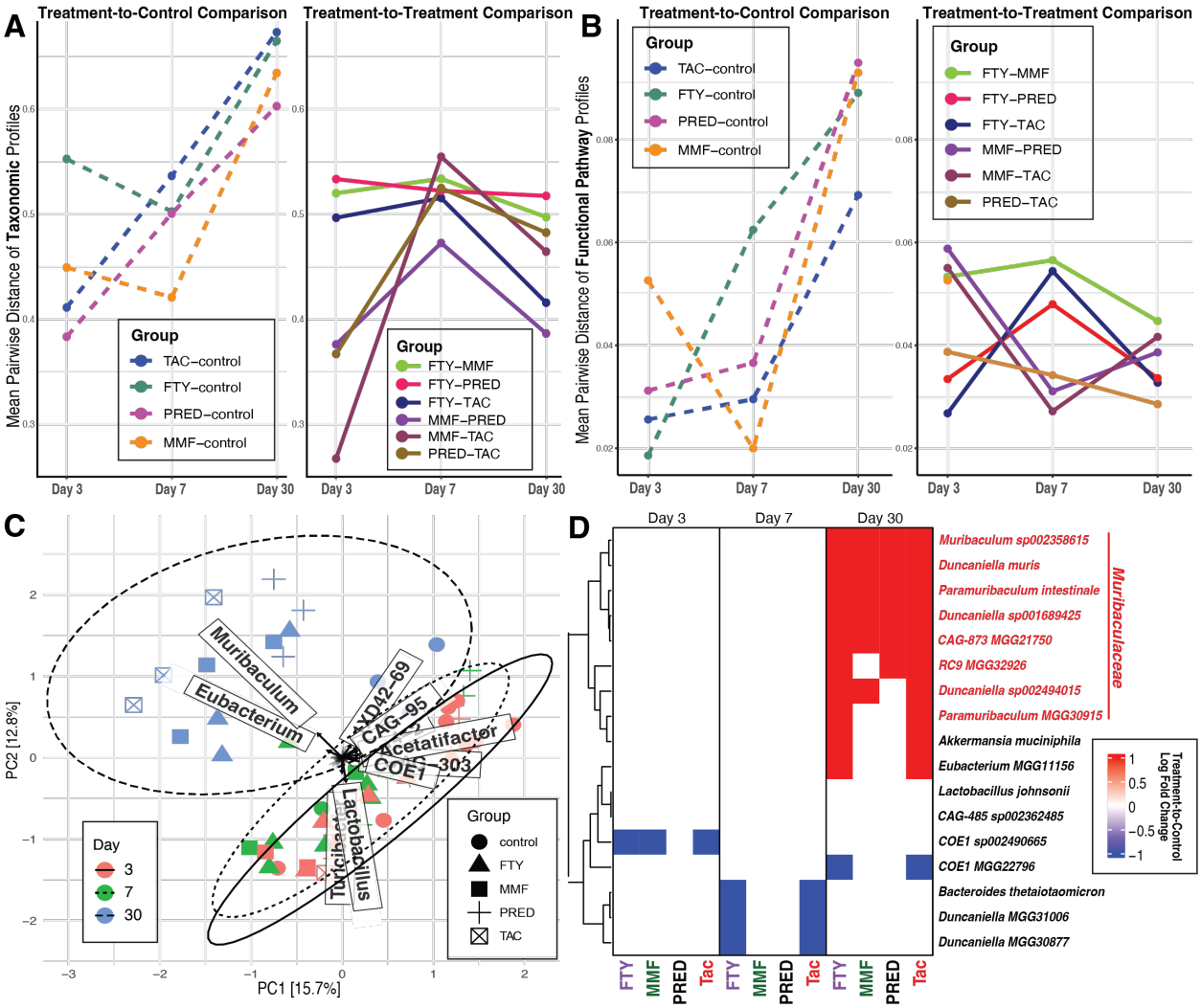


1274

1275

**Figure 2.**

**A)**

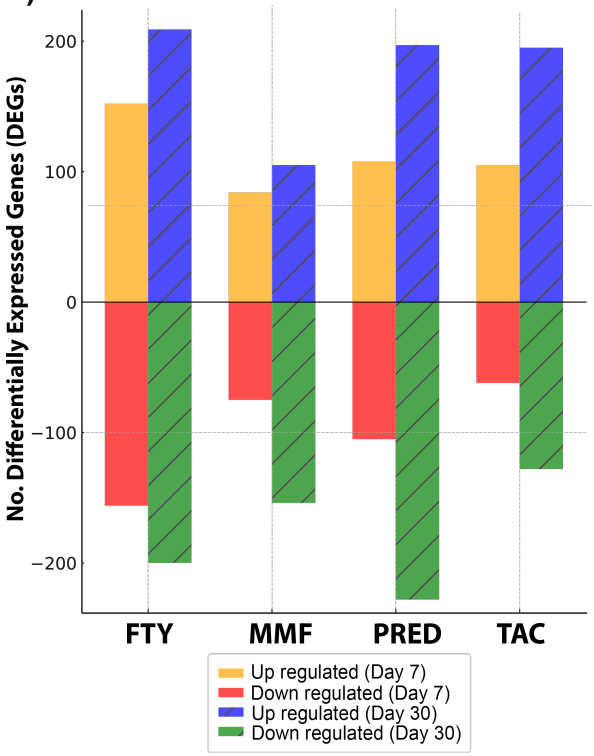
No. Differentially Expressed Genes (DEGs)
200
100
0
−100
−200
FTY
MMF
PRED
TAC
Up regulated (Day 7)
Down regulated (Day 7)
Up regulated (Day 30)
Down regulated (Day 30)

**Figure 2. B)**

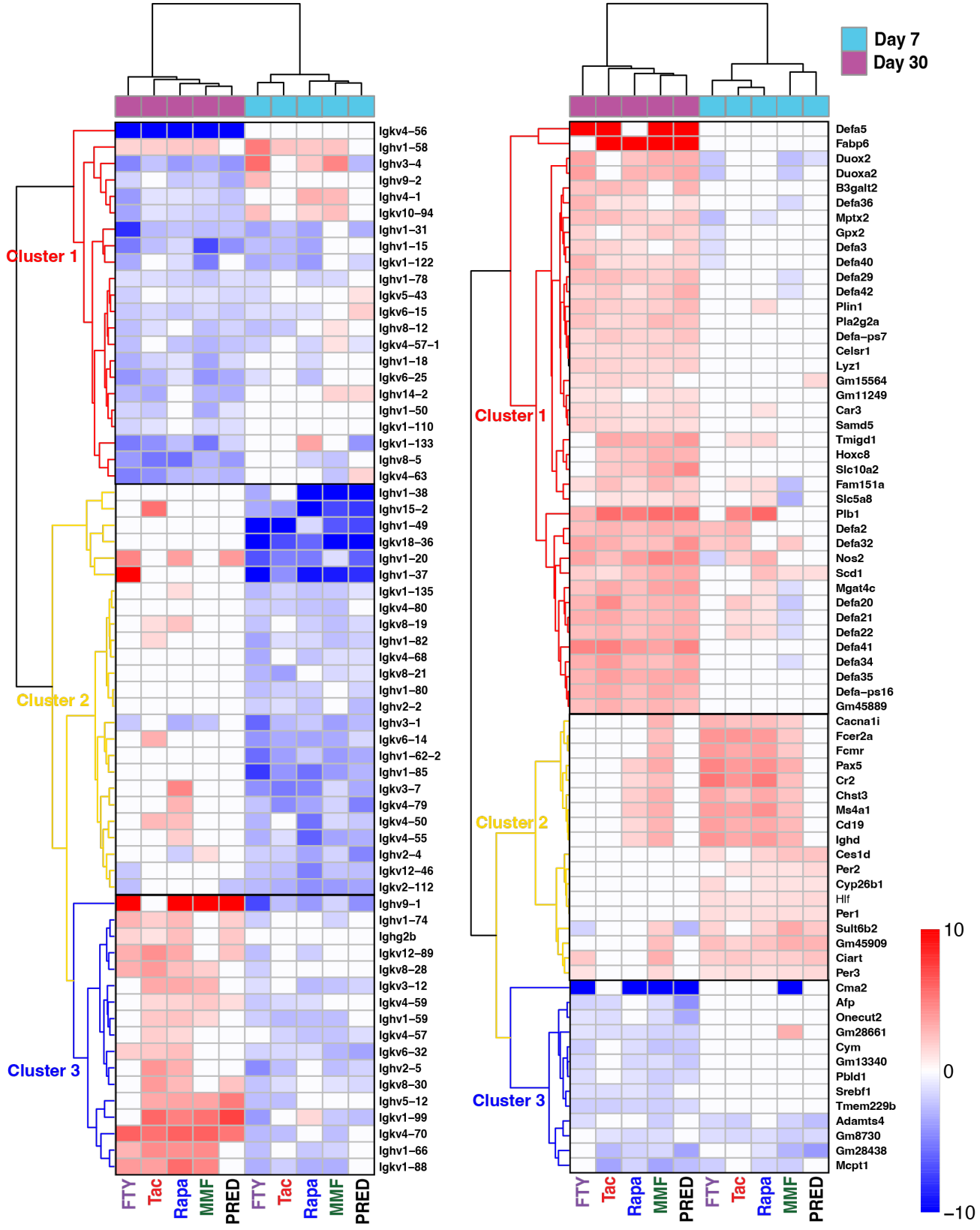
Day 7
Day 30
Cluster 1
Cluster 2
Cluster 3
Igkv4–56
Ighv1–58
Ighv3–4
Ighv9–2
Ighv4–1
Igkv10–94
Ighv1–31
Ighv1–15
Igkv1–122
Ighv1–78
Igkv5–43
Igkv6–15
Ighv8–12
Igkv4–57–1
Ighv1–18
Igkv6–25
Ighv14–2
Ighv1–50
Igkv1–110
Igkv1–133
Ighv8–5
Igkv4–63
Ighv1–38
Ighv15–2
Ighv1–49
Igkv18–36
Ighv1–20
Ighv1–37
Igkv1–135
Igkv4–80
Igkv8–19
Ighv1–82
Igkv4–68
Igkv8–21
Ighv1–80
Ighv2–2
Ighv3–1
Igkv6–14
Ighv1–62–2
Ighv1–85
Igkv3–7
Igkv4–79
Igkv4–50
Igkv4–55
Ighv2–4
Igkv12–46
Igkv2–112
Ighv9–1
Ighv1–74
Ighg2b
Igkv12–89
Igkv8–28
Igkv3–12
Igkv4–59
Ighv1–59
Igkv4–57
Igkv6–32
Ighv2–5
Igkv8–30
Ighv5–12
Igkv1–99
Igkv4–70
Ighv1–66
Igkv1–88
Defa5
Fabp6
Duox2
Duoxa2
B3galt2
Defa36
Mptx2
Gpx2
Defa3
Defa40
Defa29
Defa42
Plin1
Pla2g2a
Defa–ps7
Celsr1
Lyz1
Gm15564
Gm11249
Car3
Samd5
Tmigd1
Hoxc8
Slc10a2
Fam151a
Slc5a8
Plb1
Defa2
Defa32
Nos2
Scd1
Mgat4c
Defa20
Defa21
Defa22
Defa41
Defa34
Defa35
Defa–ps16
Gm45889
Cacna1i
Fcer2a
Fcmr
Pax5
Cr2
Chst3
Ms4a1
Cd19
Ighd
Ces1d
Per2
Cyp26b1
Hlf
Per1
Sult6b2
Gm45909
Ciart
Per3
Cma2
Afp
Onecut2
Gm28661
Cym
Gm13340
Pbld1
Srebf1
Tmem229b
Adamts4
Gm8730
Gm28438
Mcpt1
FTY
Tac
Rapa
MMF
PRED
10
0
–10

**Figure 2. C)**

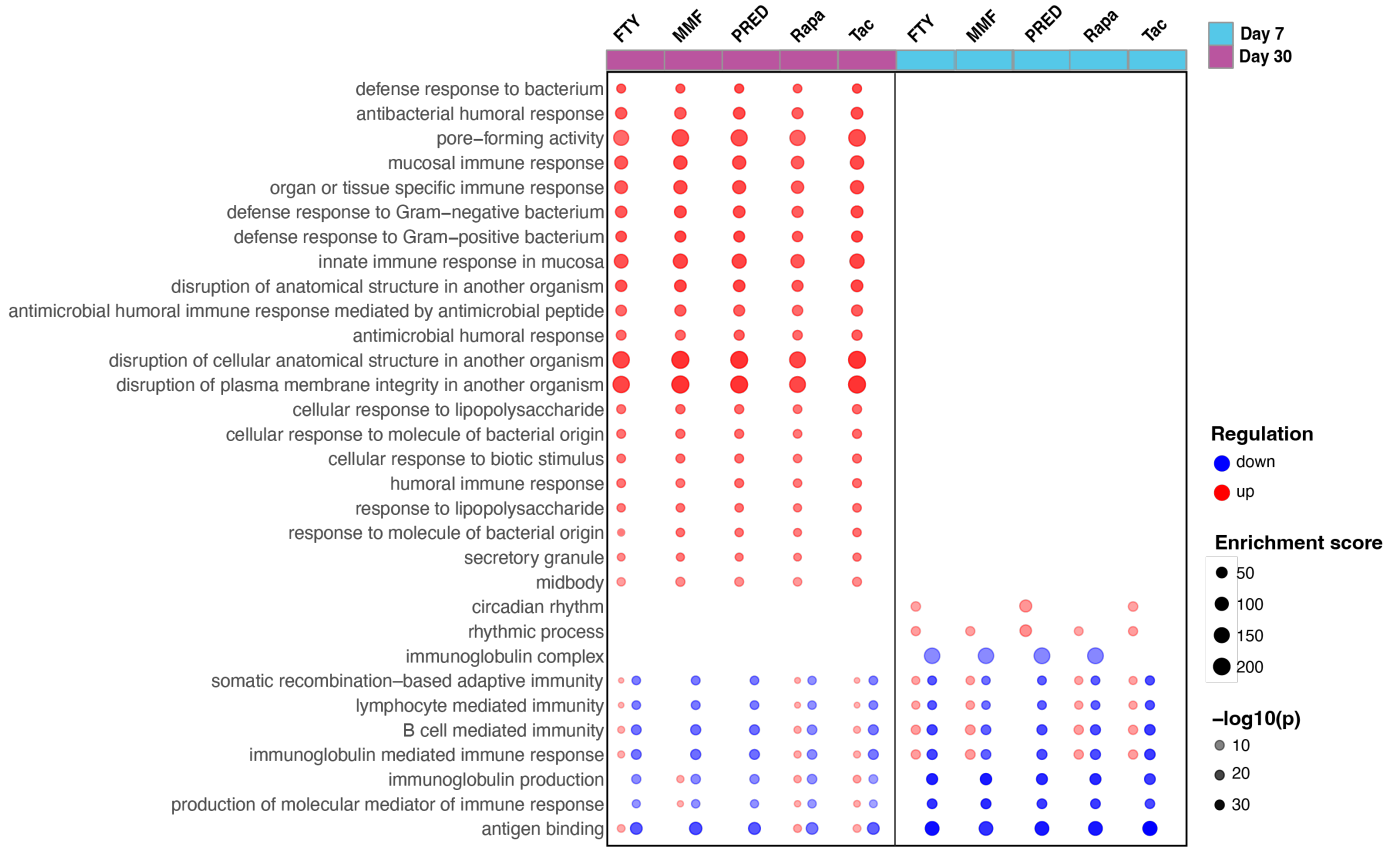
FTY
MMF
PRED
Rapa
Tac
FTY
MMF
PRED
Rapa
Tac
Day 7
Day 30
defense response to bacterium
antibacterial humoral response
pore−forming activity
mucosal immune response
organ or tissue specific immune response
defense response to Gram−negative bacterium
defense response to Gram−positive bacterium
innate immune response in mucosa
disruption of anatomical structure in another organism
antimicrobial humoral immune response mediated by antimicrobial peptide
antimicrobial humoral response
disruption of cellular anatomical structure in another organism
disruption of plasma membrane integrity in another organism
cellular response to lipopolysaccharide
cellular response to molecule of bacterial origin
cellular response to biotic stimulus
humoral immune response
response to lipopolysaccharide
response to molecule of bacterial origin
secretory granule
midbody
circadian rhythm
rhythmic process
immunoglobulin complex
somatic recombination−based adaptive immunity
lymphocyte mediated immunity
B cell mediated immunity
immunoglobulin mediated immune response
immunoglobulin production
production of molecular mediator of immune response
antigen binding
Regulation
down
up
Enrichment score
50
100
150
200
−log10(p)
10
20
30

1285 **Figure 3.**

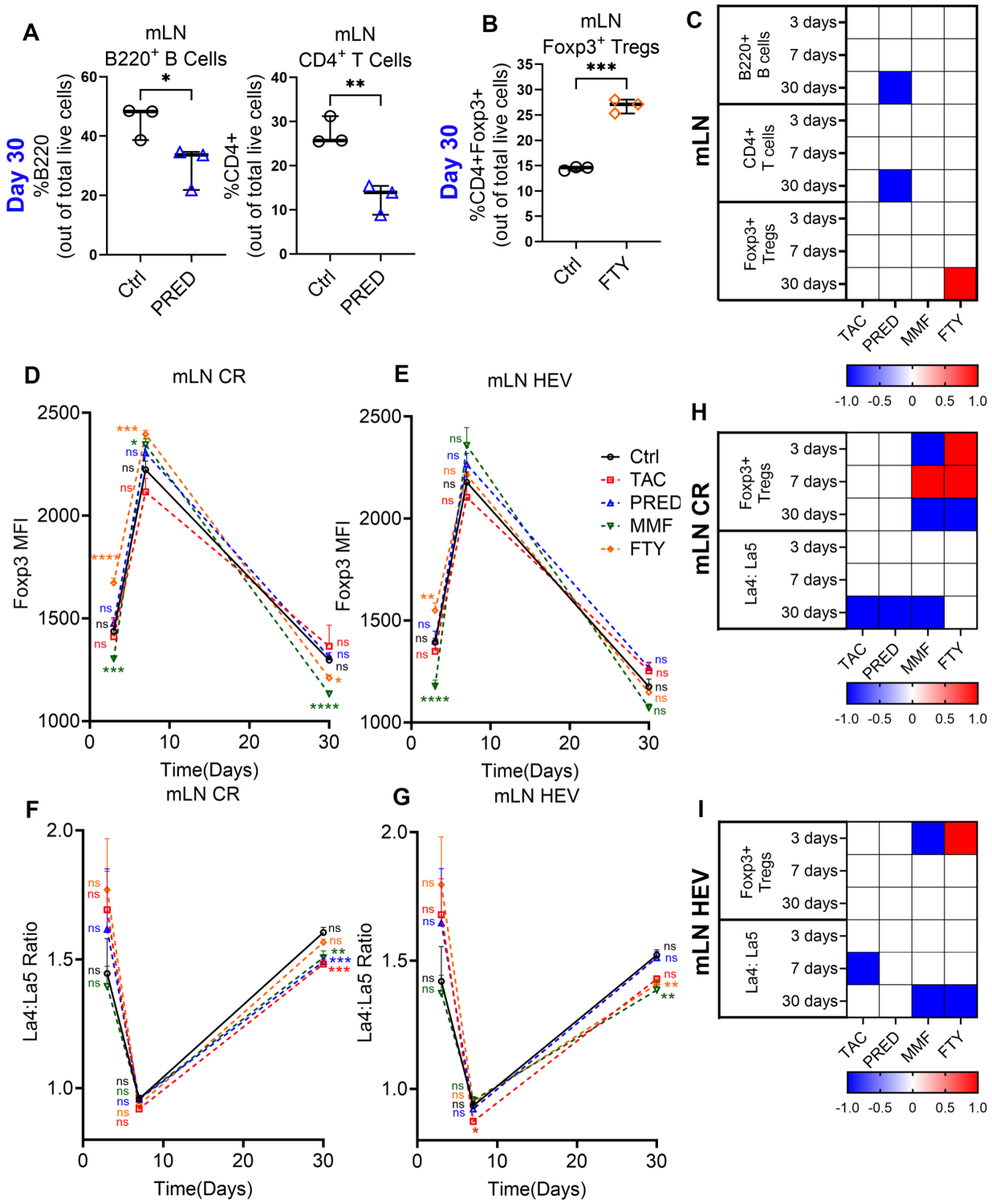


1286

1287

1288 **Figure 4.**

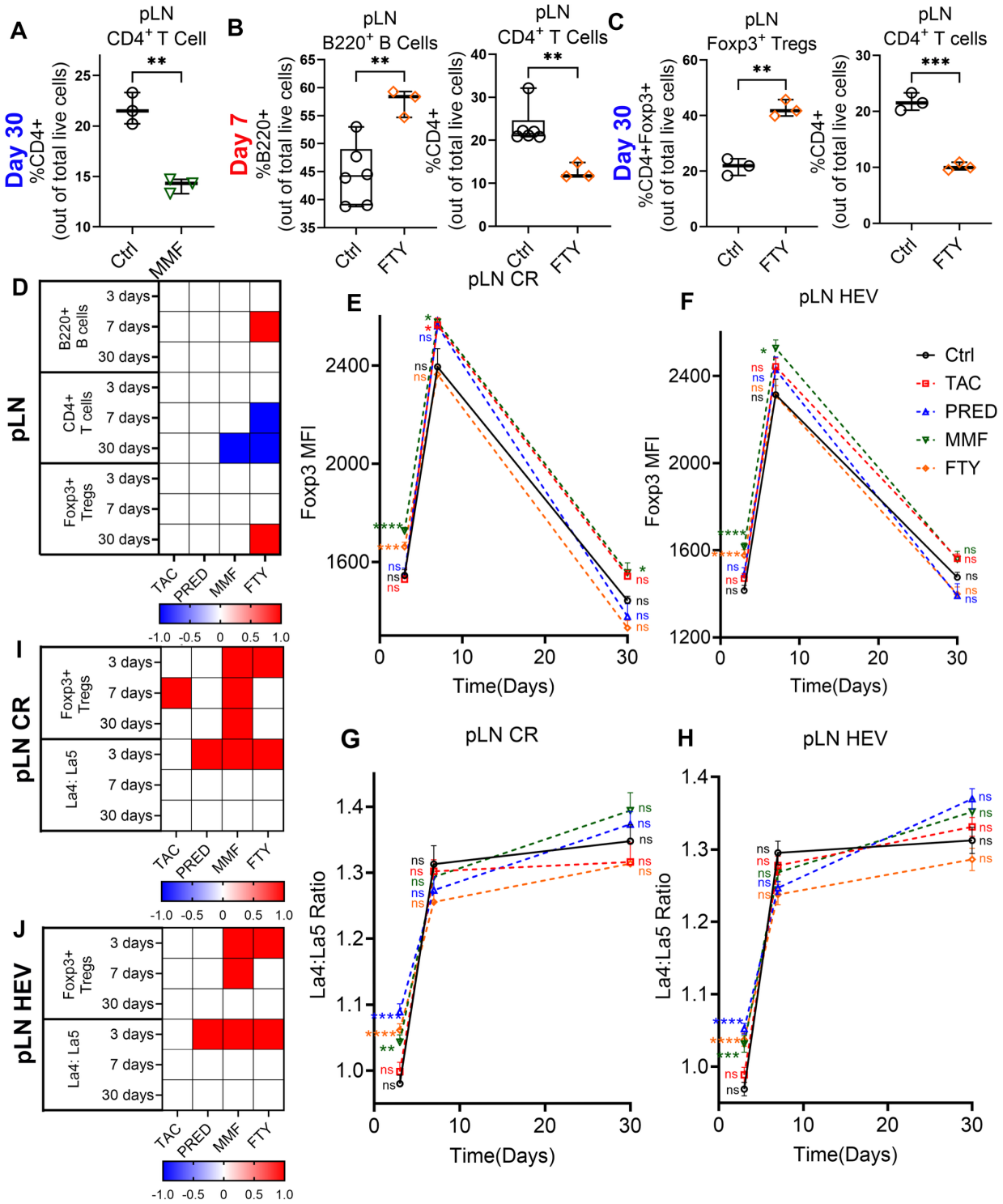


1289

1290

1291 **Figure 5.**

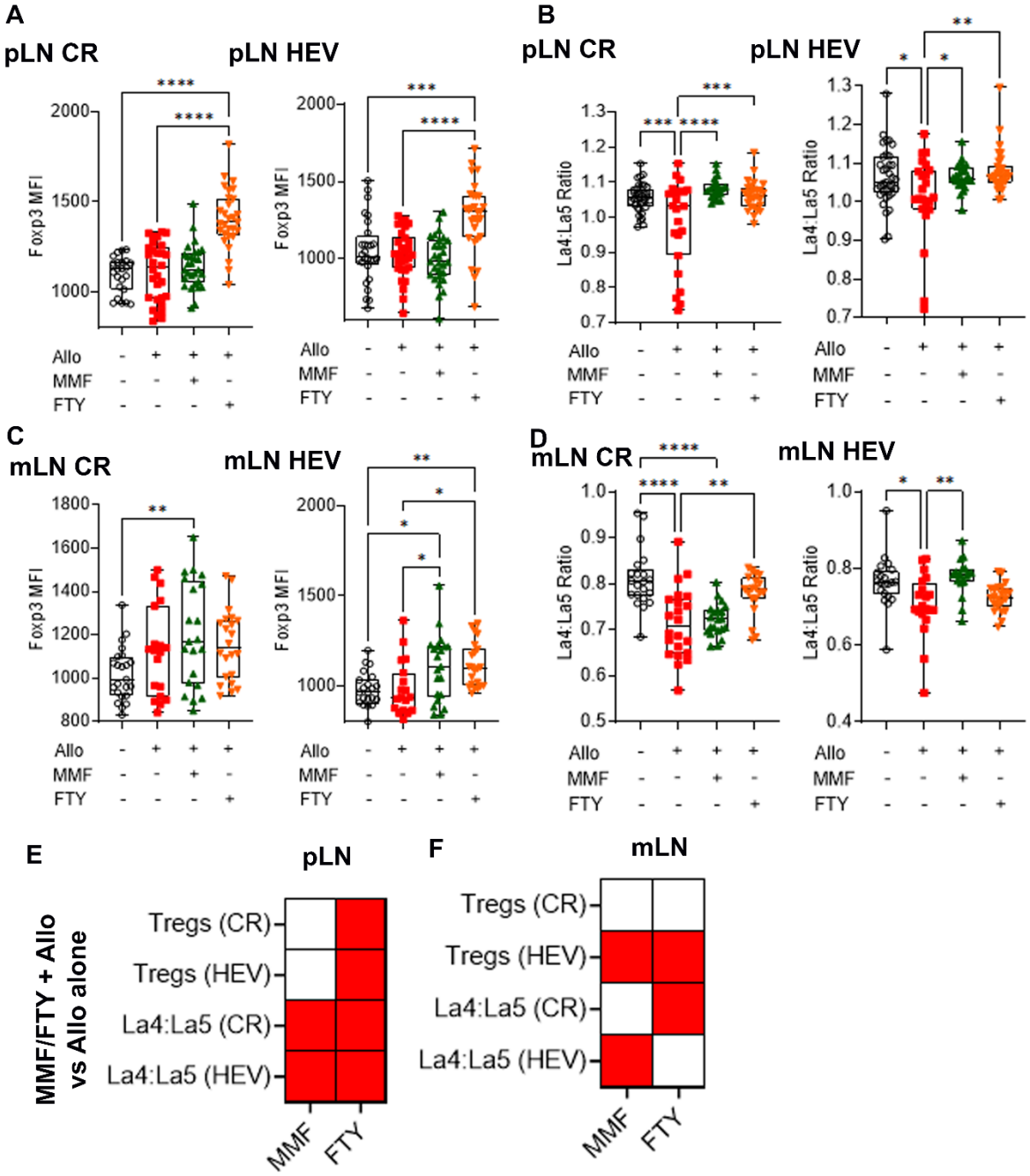


1292

1293

1294 **Figure 6.**

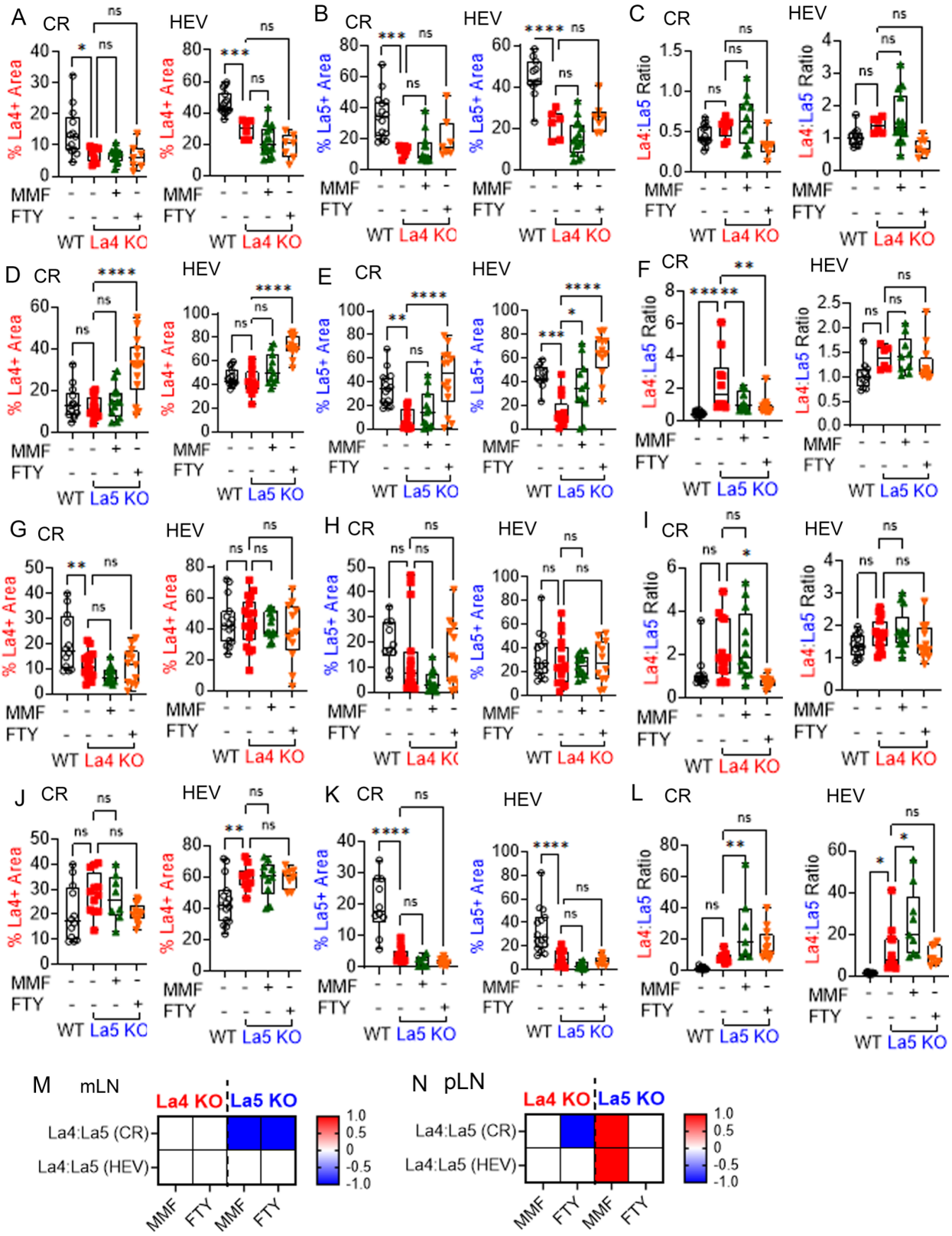
A CR HEV
% La4+ Area
MMF
FTY
WT La4 KO
B CR HEV
% La5+ Area
WT La4 KO
C CR HEV
La4:La5 Ratio
WT La4 KO
D CR HEV
% La4+ Area
WT La5 KO
E CR HEV
% La5+ Area
WT La5 KO
F CR HEV
La4:La5 Ratio
WT La5 KO
G CR HEV
% La4+ Area
WT La4 KO
H CR HEV
% La5+ Area
WT La4 KO
I CR HEV
La4:La5 Ratio
WT La4 KO
J CR HEV
% La4+ Area
WT La5 KO
K CR HEV
% La5+ Area
WT La5 KO
L CR HEV
La4:La5 Ratio
WT La5 KO
M mLN
La4 KO La5 KO
La4:La5 (CR)
La4:La5 (HEV)
MMF FTY MMF FTY
N pLN
La4 KO La5 KO
La4:La5 (CR)
La4:La5 (HEV)
MMF FTY MMF FTY

1295

1296 **Figure 7.**

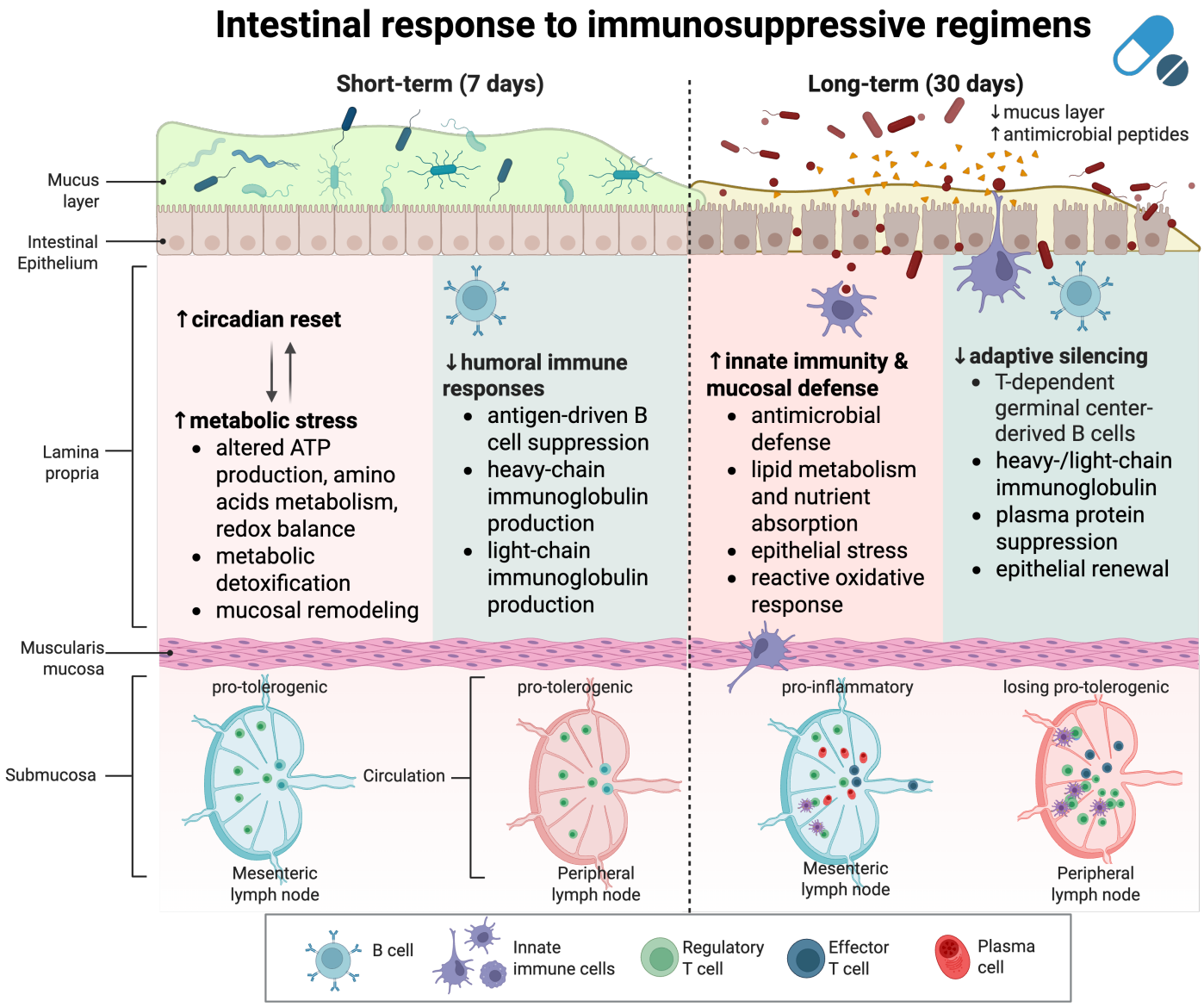


1297

1298